PONTIFICIA UNIVERSIDAD CATÓLICA DEL PERÚ

ESCUELA DE POSTGRADO

DETERMINATION OF THE OPTICAL BANDGAP OF THIN AMORPHOUS $(SiC)_{1-x}(AlN)_x$ FILMS PRODUCED BY RADIO FREQUENCY DUAL MAGNETRON SPUTTERING

Tesis para optar el Grado de Magíster en Física que presenta:

Jorge Andrés Guerra Torres

ASESOR: Dr. Roland Weingärtner

Lima, julio 2010

Este trabajo está dedicado a mis padres que crearon la vía necesaria y mis maestros que supieron guiarme a través de ella.

Determination of the optical bandgap of thin amorphous $(SiC)_{1-x}(AlN)_x$ films produced by radio frequency dual magnetron sputtering

Jorge Andrés Guerra Torres

Propuesto para el grado de magíster en Física

2010

Abstract

Amorphous wide bandgap semiconductor thin films of the pseudobinary compound $(SiC)_{1-x}(AlN)_x$ were grown by radio frequency dual magnetron sputtering on CaF_2, MgO, Al_2O_3 and glass substrates. In order to determine the optical bandgap versus composition of the film we performed spectroscopic transmission measurements from where the refractive index and absorption coefficient were calculated, and energy dispersion spectroscopy (EDS) measurements from where the composition was determined. The optical bandgap is determined for each composition from the absorption coefficient in two different ways: according to the Tauc plot and using the $(\alpha h\nu)^2$ plot. The dependence of the optical bandgap on the composition x can be described by Vegard's empirical law for alloys.

Resumen

Películas delgadas amorfas semiconductoras de amplio ancho de banda del compuesto pseudobinario $(SiC)_{1-x}(AlN)_x$ fueron depositadas por pulverización por un sistema de dos magnetrones de radio frecuencia sobre CaF_2, MgO, Al_2O_3 y vidrio. Con el fin de determinar el ancho de banda óptico versus la composición de la película, se realizaron medidas espectroscópicas de la transmisión de donde el índice de refracción y el coeficiente de absorción fueron calculados y medidas espectroscópicas de la dispersión de energía (EDS) de donde la composición fue determinada. El ancho de banda óptico es determinado para cada composición a partir del coeficiente de absorción de dos maneras distintas: según el gráfico de Tauc y utilizando el gráfico de $(\alpha h\nu)^2$. la dependencia del ancho de banda con la composición x puede ser descrita por la ley empírica de Vegard para aleaciones.

Acknowledgments

This research is funded by the Deutsche Forschungsgemeinschaft (DFG) and the Bundesministerium für Zusammenarbeit und Entwicklung (BMZ) under contract number WI393-20-1,2, WI393/21-1,2,3 and is supported by the German Academic Exchange Service (DAAD) under contract numbers D/05/12207 and D/08/09227

Index

Chapter I

Introduction

Wide bandgap semiconductors have been of increasing interest for photonic applications in the last decade [1]. This is mainly due to properties like their high breakdown voltage and thermal conductivity. Their amorphous counterparts (i.e. *a*-SiC and *a*-AlN) have the advantage to be produced rather simply and inexpensively without the drawback of losing those important properties. In addition, there are further aspects which are missing in the crystalline state. For example, the indirect character for optical transitions in *c*-SiC is absent in the amorphous state, so that applications in optoelectronics seem promising. In the case of *a*-AlN even applications in the near ultraviolet region are possible, due to the wide optical bandgap of 5.61 eV [2]. In the framework of a research project running at the PUCP, Physics section, in collaboration with The University of Erlangen-Nürnberg, amorphous $(SiC)_{1-x}(AlN)_x$ thin films were grown on glass, CaF_2, MgO and Sapphire substrates. In principle *a*-$(SiC)_{1-x}(AlN)_x$ has the same potentials of applications. However, the engineering of the bandgap by variation of the composition *x* opens the possibility to tailor physical properties in an essential way [3][4], e. g., the emission from rare earth doped *a*-$(SiC)_{1-x}(AlN)_x$ can be optimized [5].

It is important to remark that the properties of the *a*-$(SiC)_{1-x}(AlN)_x$ films behave as the properties of a compound and not as a composite in the sense that the solid solution has properties different from the properties of the constituent materials. I. e. the optical bandgap that determines the optical properties of the material will change fundamentally with the composition and not as a superposition of the optical bandgaps of SiC and AlN.

An overview of the theory behind the covalent bonding will be presented at the first section of the chapter two, from this point the emergence of a bandgap without taking into account the structural arrangement of the atoms in a solid will be shown, closing this section an example of the similitude in the optical properties between amorphous and crystalline Silicon will be shown. In the second section of the chapter two, the

theory of the fundamental absorption of crystalline and amorphous solids will be presented because of the extent of the topic and its importance for the later experimental work this section will contain detailed calculations of the fundamental absorption divided in three main cases. First the fundamental absorption of a direct crystal at zero Kelvin temperature. Second the fundamental absorption of a direct crystal at a finite temperature and finally an approach to the fundamental absorption of amorphous solids.

The details of the experiments performed will be presented in the chapter three, this will cover details of the film growing method, the composition measure, the annealing treatments and details of the transmission measurements.

The optical constants determination method and therefore the bandgap determination will be presented in the chapter four. In this chapter the most common method to calculate the optical constants of a solid using a single transmission measurement will be presented and explained in detail. In the subsequent section a variation of the later method will be proposed and applied in the particular case of the films produced in our laboratories.

In the last chapter, comprehensive measurements of the bandgap of thin a-$(SiC)_{1-x}(AlN)_x$ films for the whole composition range are shown. The shift of the bandgap and the shift of the low energy absorption, the band tails due to annealing treatments are also investigated up to temperatures of 700°C.

Chapter II

Theoretical background

Amorphous materials have attracted attention in the last two decades [1-6]. As it was mentioned before in the first chapter the principal reason is their industrial potential of applications. At the same time there is a lack of understanding of their materials properties [6], which are different from those of crystalline state. Some properties vary even for samples of the same material.

In this chapter the basic theory to understand the fundamentals of bandgap engineering with a-$(SiC)_{1-x}(AlN)_x$ will be provided. First we will present the theory of the energy bands of solids, explaining how it is formed starting from the covalent bonding. Later on, the fundamental absorption for crystalline solids is presented and described at zero Kelvin temperature and for finite temperatures. We address the most common and well known approach for the fundamental absorption of amorphous solids developed by J. Tauc [7].

Energy bands in solids

Before pretending to do bandgap engineering of an amorphous compound it is important to understand the differences of the fundamental absorption between crystalline and amorphous semiconductors materials. For this, it is necessary to understand the electronic energy bands and their structure. The origin of the bandgap does not lay in the material structure order but in the chemistry of their bonds [6]. That is why we first introduce the concept of covalent bonding in solids and molecules, starting with the simplest example, two atoms forming a covalent bond and then defining the so called bandgap in solids.

The covalent bond in solids and molecules

The interaction between the closest neighbors is the one of most importance in the covalent bonding. Let us take for example a diatomic molecule conformed by two atoms *A* and *B* separated by a distance *R* (see fig. 1). The characteristics of the bonding can be obtained from the quantum theory of chemical bonding [6][8].

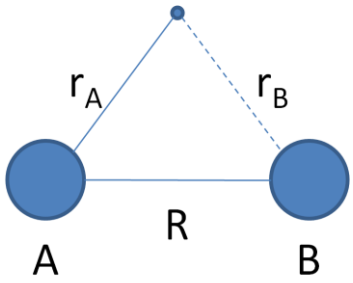

Figure 2.1.1: Schematic representation of a diatomic molecule where the atoms A and B are separated by a distance R and share one electron to form a covalent bond.

To write the Hamiltonian let us name the wave functions that represent the state of one electron in the occupied valence state ϕ_A and ϕ_B for each atom, respectively. Therefore we can write the Hamiltonian as

$$H = -\frac{\hbar^2}{2m_e}\nabla^2 - k\left[-\frac{ze^2}{r_A} - \frac{ze^2}{r_B} + \frac{z^2e^2}{R}\right] \tag{2.1.1}$$

Where $k = 1/4\pi\epsilon_0$, z is the number of electrons in the valence band and m_e the electron mass.

The solution of the Schrödinger equation $E\psi = H\psi$, can be written as equation (2.1.2).

$$E = \frac{\int \psi * H\psi d^3\boldsymbol{r}}{\int \psi * \psi d^3\boldsymbol{r}} \tag{2.1.2}$$

Now, we will follow the LCAO (Linear Combination of Atomic Orbitals) method, where we assume the molecular orbital ψ as a linear combination of the electron wave functions of the individual atoms (i.e. ϕ_A, ϕ_B). Replacing

$$\psi = c_A\phi_A + c_B\phi_B \tag{2.1.3}$$

into (2.1.2) we get for the energy,

$$E = \frac{c_A^2 H_{AA} + c_B^2 H_{BB} + 2c_A c_B H_{AB}}{c_A^2 + c_B^2 + 2c_A c_B S} \tag{2.1.4}$$

With the abbreviations

$$H_{AA} = H_{BB} = \int \phi_A^* H \phi_A d^3\boldsymbol{r} = \int \phi_B^* H \phi_B d^3\boldsymbol{r}$$

$$H_{AB} = H_{AB} = \int \phi_A^* H \phi_B d^3\boldsymbol{r} = \int \phi_B^* H \phi_A d^3\boldsymbol{r}$$

$$S = \int \phi_A^* \phi_B d^3\boldsymbol{r}$$

Minimizing then the energy E respect to the coefficients c_A y c_B we obtain two solutions, E_+ y E_- as energy auto values for the molecular orbital separated by $\Delta E = E_- - E_+$.

$$E_\pm = \frac{H_{AA} \mp H_{AB}}{1 \mp S} \tag{2.1.5}$$

The obtained result in the equation (2.1.5) is well known in quantum chemistry, it indicates that the energy state of an isolated atom is divided in two energy levels when two atoms are brought close together and interact. The lowest energy state is known as bonding orbital and its energy is lower than the energy of the state of isolated individual atoms. The higher energy is called anti-bonding orbital [6][8].

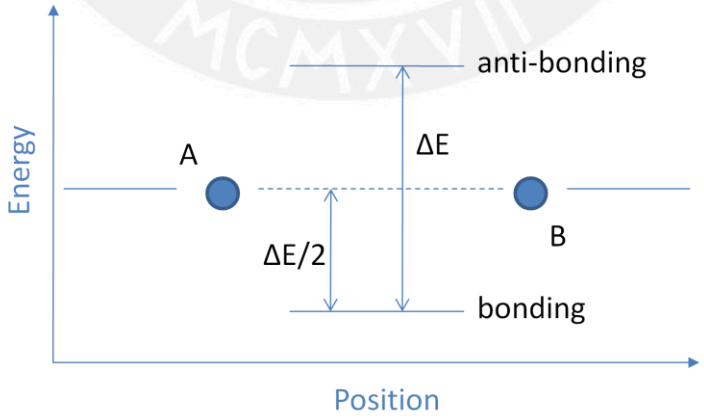

Figure 2.1.2: Representation of the bonding and anti-bonding of two atoms when they are brought together to form a covalent bond. When the bond is made two new energy levels are formed.

The electronic states can contain maximal two electrons. If both atoms contribute with one electron then both electrons will occupy the lower state and therefore will form a bond. However, it is not possible to identify which electron belongs to which atom, the orbital bonding state is a state of the diatomic system and not of an individual atom. The electrons are indistinguishable particles. The terms H_{AB} and S depend on the inter-atomic distance R and if $R \to \infty$ both H_{AB} and S became zero, thus the energy separation of the bonding and anti-bonding states is reduced when the distance R increases.

The LCAO can be expanded to determine the electronic energy states in semiconductors that usually consist on a large number of atoms. In this case the LCAO is known as *Tight Binding Model*. The separation between the bonding orbital and anti-bonding orbital is filled with quite closed energy states, each one due to each atom in the solid. So in solids each atomic energy state is grouped in an energy band. In the next section we will develop this idea taking an example and we will define the energy bandgap and the kinds of solids from the shape of their energy bands.

Electronic states in crystalline and amorphous materials

Let us take a solid made by N atoms, for example carbon atoms with the $2\boldsymbol{s}^2 2\boldsymbol{p}^2$ configuration of occupation. When the atoms are brought together, the overlap of their electronic wave functions causes that the s and p orbitals mix with each other and became one band with a capacity of $2N(s) + 6N(p) = 8N$ electrons, see the figure (2.2.1). The band is then not completely occupied, therefore a solid formed in this way should behave as a conductor because electrons of partially filled bands contribute to an electrical current [6][9].

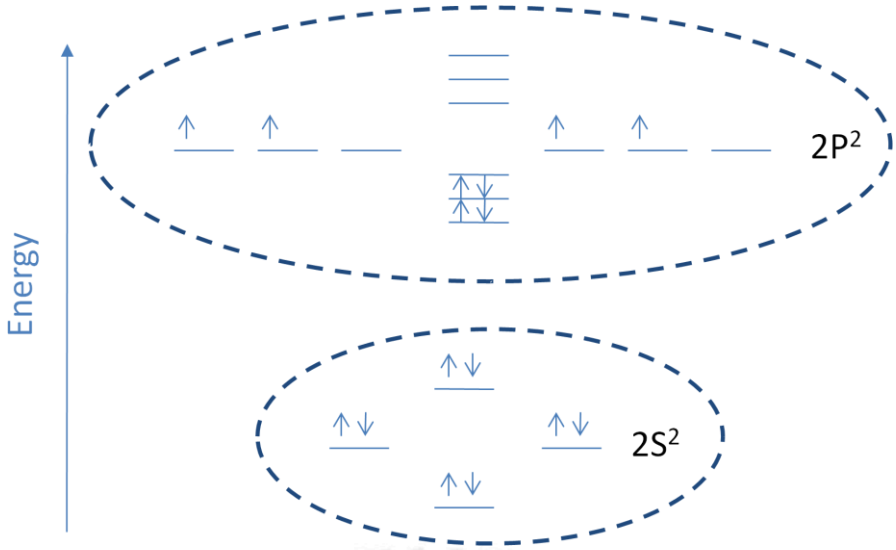

Fig. 2.2.2: Representation of the $2\boldsymbol{s}^2$ and $2\boldsymbol{p}^2$ overlapped orbitals (following LCAO). The orbitals are not completely occupied and therefore a solid formed in this way should behave as a conductor.

However, in the case of the diamond this is not true, diamond is an insulator. This is caused by the $\boldsymbol{sp}^3$ hybridization of the carbon atoms which increases the orbitals and therefore the overlap, lowering the energy. The orbitals are directed towards the corners of the tetrahedron. The band with a capacity of $8N$ electrons we describe earlier is divided in two separated bands each with a capacity of $4N$ electrons, the lower band is filled completely with the four available electrons per atom from the $\boldsymbol{sp}^3$ hybridization and the upper energy band remains empty [6][10] (see fig. 2.2.3). Both bands get separated by an energy gap ΔE the bandgap that depends on the interatomic separation.

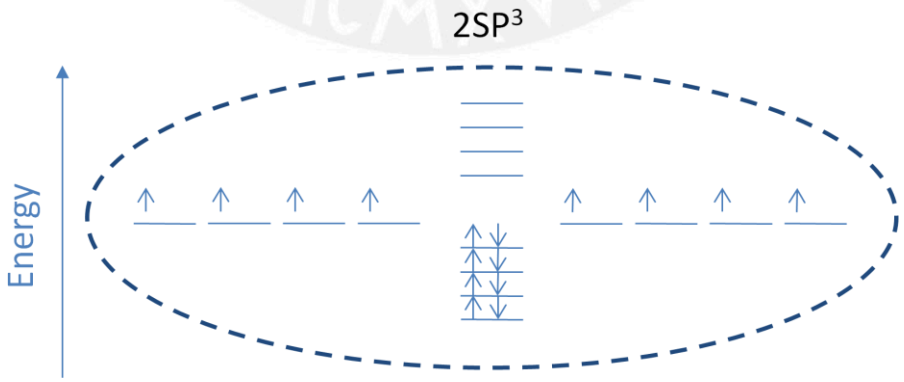

Fig. 2.2.3 Representation of the energy levels formed by the $\boldsymbol{sp}^3$ hybridization, i.e. the diamond, in this case due to the hybridization the behavior is that of an isolator

Depending on the size of the gap and the occupation grade (or Fermi level) a solid formed in this way will behave as an isolator (i.e. the diamond) or as a semiconductor (i.e. Si, Ge, etc.). It is important to remark that the above description is valid for crystalline and amorphous solids, since we didn't use the translational symmetry of a crystal and therefore the formation of a bandgap in either crystalline or amorphous solids is justified.

The electronic wave function of a solid can be written following the LCAO theory for many atoms as (2.2.1.1).

$$\psi_i(r) = \sum_n C_n \phi_i(r - r_n) \qquad (2.2.1.1)$$

Where $\phi_i(r - r_n)$ represents the electronic wave function of the i-*th* state of an atom located at r_n and with C_n the linear combination coefficient. In principle the equation (2.2.1.1) is applicable to both *a*- and *c*- solids but it is only in the crystalline where the coefficient C_n can be written by $C_n = N^{1/2} e^{i\boldsymbol{k}\cdot\boldsymbol{r}_n}$ due to the translational symmetry, where $\boldsymbol{k}$ is the electronic wave vector. As C_n is a Bloch wave, the charge carrier is delocalized through the whole crystal.

The electronic wave functions for a crystalline solid, these are the so called Bloch functions, and the electronic energy bands can be obtained as function of the wave vector $\boldsymbol{k}$. The top higher energy band is known as conduction band (c.b.) and the bottom filled band is called valence band (v.b.), both separated by the energy gap $\Delta E = E_g$ that depends also on the wave vector $\boldsymbol{k}$. This gives arise to two kinds of crystalline solids, one in which the absolute maximum of the valence band and the absolute minimum of the conduction band are found to be at the same wave vector $\boldsymbol{k}$, called direct bandgap solid, all other cases are called indirect bandgap solid. Every electronic transition between bands in these solids must obey the momentum conservation [6][9].

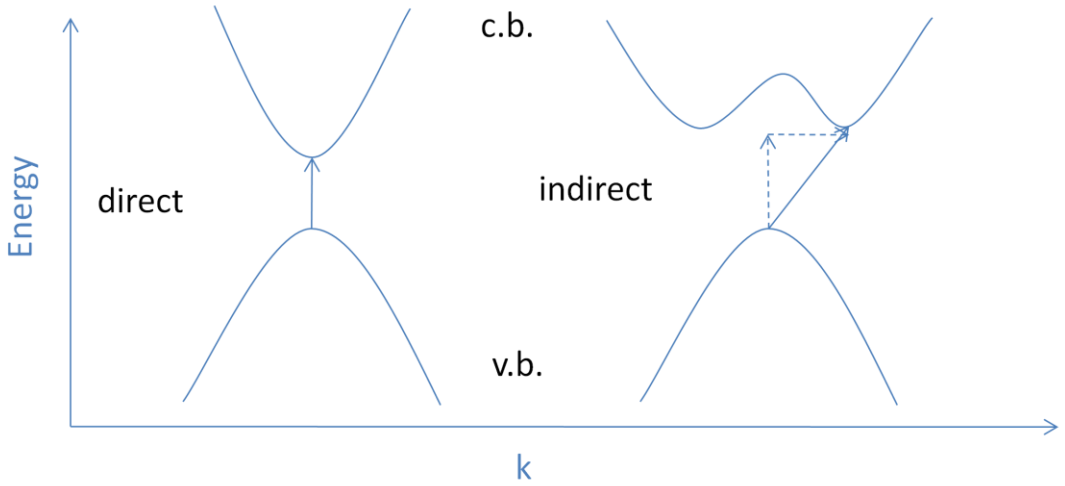

Fig. 2.2.4 Schematic representation of the energy dispersion versus the wave vector ***k*** for direct and the indirect bandgaps.

In the case of amorphous solids, the inexistence of long range order does not allow such distinction between solids based on the electron dispersion, because the wave vector is not a good quantum number. However the interaction of so many atoms allows the formation of quasi-continuum states and therefore as it was proved by Weaire and Thorpe (1971) through the *tight binding model*, a discontinuity in the electronic density of states of solids is found separating the valence and conduction bands and thus leading to the formation of a bandgap. These quasi-continuum states are known as valence and conduction extended states due to the fact that there is no long range order (and ***k*** is not a good quantum number) for describing the bands in amorphous solids [6][11]. The description of the bands is an extension of the theory in the crystalline case. They are also called delocalized states, but this name can always be applied when an electronic wave function is not bounded and this happens in the crystalline and amorphous solids, in the first with the Bloch waves, and in the second the electronic waves are electronic waves with a wavelength much longer than the average crystal size and therefore it can be treated as if it is not bounded but delocalized. Thus amorphous solids have in many cases a similar behavior as their crystalline counterpart [12]. In fact this can be seen when we compare for example the absorption coefficient of *a*-Si:H at different Hydrogen concentrations and *c*-Si at different temperatures, see fig. (2.2.5).

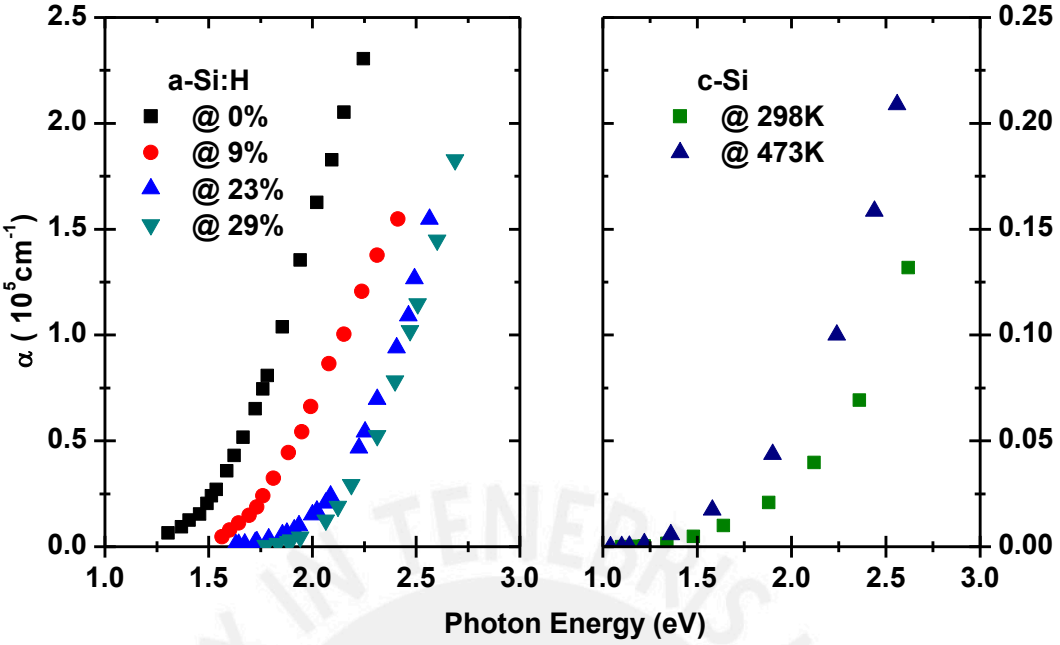

Fig. 2.2.5: Left, absorption coefficient plotted versus energy of four different samples of *a*-Si:H differing on the hydrogen concentration. Right, absorption coefficient plotted versus energy of a *c*-Si sample measured at two different temperatures. (Demichellis *et al.*, 1986)

The similarities between crystalline and amorphous semiconductors suggest apply the band scheme of the former on the latter [12]. It can also be observed from the figure (2.2.5) that the increment of temperature produces and enhancement of the tail in the crystalline case, while in the amorphous case this tail is reduced with an increment in the concentration of the hydrogen in the lattice. In the next section we will need these observations.

Fundamental absorption

In amorphous semiconductors the optical properties are of great importance. This is mainly due to the fact that the optical properties are directly related to structural and electronic properties of any solid and therefore are very important in device development [6][11][12].

In the next subsections the theory of the fundamental absorption for crystals will be developed at zero Kelvin temperature and for higher temperatures. Finally, we close this section with an approach to the fundamental absorption of amorphous semiconductors

that only takes into account transitions between extended states developed by J. Tauc [7].

Fundamental absorption in direct crystals at zero Kelvin temperature

The absorption coefficient in the fundamental absorption region is directly related to the optical bandgap of solids and its measuring is relatively simple using a spectrophotometer. In this section we will derivate an expression for the fundamental absorption in crystalline solids at cero Kelvin temperature. First we will start from a semi-classic approach to derivate the Hamiltonian that describes the electromagnetic interaction between the electromagnetic radiation and the Bloch electrons inside a semiconductor. Then, we will relate the transition rate between the valence and conduction bands with the absorbed energy by the solid. Finally using perturbation theory we derivate the fundamental absorption as a function of the photon energy.

The electromagnetic field is treated classically while the electrons are described by the Bloch waves.

$$H = \frac{1}{2m}[\boldsymbol{p} + e\boldsymbol{A}]^2 + V(r) \qquad (2.2.1.1)$$

Where $\boldsymbol{p}$ is the free electron momentum, $\boldsymbol{A}$ is the vector potential of the electromagnetic field, m is the free electron mass and $V(r)$ is the periodic potential of the crystalline semiconductor.

Developing the quadratic term in the equation (2.2.1.1) considering $\boldsymbol{p}$ and $\boldsymbol{A}$ quantum mechanic operators that is i.e. "$\boldsymbol{p} = -i\hbar\boldsymbol{\nabla}$".

$$[\boldsymbol{p} + e\boldsymbol{A}]^2 = \boldsymbol{p}^2 + e\boldsymbol{A}\cdot\boldsymbol{p} + e\boldsymbol{p}\cdot\boldsymbol{A} + e^2\boldsymbol{A}^2 \qquad (2.2.1.2)$$

Using the Coulomb Gauge $\boldsymbol{\nabla}\cdot\mathbf{A} = 0$ we see that $[\boldsymbol{p}, \boldsymbol{A}] = 0$, where $[,]$ is the commutation operator, and therefore $e\boldsymbol{A}\cdot\boldsymbol{p} + e\boldsymbol{p}\cdot\boldsymbol{A} = 2e\boldsymbol{p}\cdot\boldsymbol{A}$ in equation (2.2.1.2). We can also neglect the term that depends quadratically on the field, $\boldsymbol{A}^2 \approx 0$ since we are dealing with small amplitudes. Under these assumptions we can rewrite the total Hamiltonian as

$$H = \frac{\boldsymbol{p}^2}{2m} + V(r) + \frac{e\boldsymbol{p}\cdot\boldsymbol{A}}{m}$$
$$H = H_0 + \frac{e\boldsymbol{p}\cdot\boldsymbol{A}}{m} \qquad (2.2.1.3)$$

The term $e\boldsymbol{p}\cdot\boldsymbol{A}/m$ is the perturbation due to the electromagnetic radiation on the solid. We call the former term $H_{eR} = e\boldsymbol{p}\cdot\boldsymbol{A}/m$.

In the light absorption process the energy is absorbed by the material through the electrons that are excited from the valence band to the conduction band. The energy density absorbed by the material must be equivalent to the energy density lost by the electromagnetic wave. Using the electronic transitions we can define the energy density rate as $W_M = R_{cv}\hbar\omega$ with R_{cv} the transition rate per volume unit between the valence and conduction bands, and $\hbar\omega$ the photon energy. The energy density rate per unit volume of the electromagnetic wave can be written as $W_R = -d\langle U\rangle/dt$ with $\langle U\rangle$ the energy density of the electromagnetic wave.

Both rates must be equal $W_M = W_R$ due to the energy conservation. We need to introduce the absorption coefficient in the equation to relate it to the photon energy. We know that the light intensity I is related to the energy density of the electromagnetic wave by $I = c/n\,\langle U\rangle$ with n the refractive index of the media where the light travels. We also know that the light intensity can be written as function of the absorption coefficient by the Lambert-Beer law as $I = I_0 e^{-\alpha x}$. Thus we can then write W_R as

$$W_R = -\frac{n}{c}\frac{dI}{dt} = -\frac{n}{c}\frac{dI}{dx}\frac{dx}{dt} \qquad (2.2.1.4)$$

We use the Lambert-Beer law to write $dI/dx = -\alpha I$ and $dx/dt = c/n$. Taking into account that the light intensity is $I = (cn\epsilon_0/2)E_0^2$ where ϵ_0 is the electric permittivity constant in the vacuum and E_0 is the electric field amplitude. Then we can relate W_R with the absorption coefficient (see equation 2.2.1.5).

$$W_R = \alpha\frac{cn\epsilon_0}{2}E_0^2 \qquad (2.2.1.5)$$

From the energy balance between the energy loss by the electromagnetic wave W_R and the energy absorbed by the material W_M, we get a relation between the absorption coefficient and the transition rate per unit volume R_{cv} (see equation 2.2.1.6).

$$\alpha \frac{c\, n\, \epsilon_0}{2} |E_0|^2 = R_{cv} \hbar\omega \tag{2.2.1.6}$$

We know that $\alpha = \omega\epsilon_i/nc$ with ϵ_i the imaginary part of the material electric permittivity coefficient ($\tilde{\epsilon} = \epsilon_r + i\epsilon_i$), replacing this into the equation (2.2.1.6) we obtain ϵ_i as function of the transition rate.

$$\epsilon_i = \frac{2\hbar}{\epsilon_0} \frac{R_{cv}}{|E_0|^2} \tag{2.2.1.7}$$

The transition rate can be written as $R_{cv} = dP_{cv}/dt$ with P_{cv} the transition probability between the valence and conduction bands. To find P_{cv} we appeal to the time dependent perturbation theory in quantum mechanics which gives the transition probability to first order correction [13]

$$P_{cv} = \frac{1}{\hbar^2} \left| \int_0^t dt' \, \mathrm{H}_{cv}(t') e^{\frac{i(E_c - E_v)}{\hbar} t'} \right|^2 \tag{2.2.1.8}$$

Where $\mathrm{H}_{cv} = \langle c|H_{eR}|v\rangle$ is the matrix element of the perturbative Hamiltonian, in this case the radiation interaction and $|\mathrm{v}\rangle$ and $|\mathrm{c}\rangle$ the stationary Bloch states of the valence and conduction bands, respectively.

$$\begin{aligned} |c\rangle &= u_{c,k_c} e^{i(\boldsymbol{k_c}\cdot\boldsymbol{r})} \\ |v\rangle &= u_{v,k_v} e^{i(\boldsymbol{k_v}\cdot\boldsymbol{r})} \end{aligned} \tag{2.2.1.9}$$

To calculate the integral in equation (2.2.1.8) let us proceed in the following way. First we write the vector potential as a function of the electric field according to reference [9] and then we will develop explicitly H_{cv}. The vector potential of the interaction term can be written as the equation (2.2.1.10) with $\boldsymbol{A} = A\hat{\mathrm{e}}$, $\hat{\mathrm{e}}$ is a unit vector in the direction of the radiation.

$$A = -\frac{E_0}{2i\omega}\left\{e^{i(\boldsymbol{q}\cdot\boldsymbol{r}-\omega t)} - c.c.\right\} \qquad (2.2.1.10)$$

With the equations (2.2.1.9) the matrix element H_{cv} is written in equation (2.2.1.11) where Ω is the volume of the unit cell.

$$\mathrm{H}_{cv} = -\frac{E_0}{2i\omega}\frac{e}{m}\frac{1}{\Omega}\int d\boldsymbol{r}\, u^*_{c,k_c}\, e^{-i\boldsymbol{k_c}\cdot\boldsymbol{r}}\left\{e^{i(\boldsymbol{q}\cdot\boldsymbol{r}-\omega t)} - c.c.\right\}\{\hat{\mathrm{e}}\cdot\boldsymbol{p}\}u_{v,k_v}e^{-i\boldsymbol{k_v}\cdot\boldsymbol{r}} \qquad (2.2.1.11)$$

The transition probability in equation (2.2.1.8) presents two similar terms when inserting the expression (2.2.1.11) resulting in (2.2.1.12).

$$P_{cv} = \left(\frac{E_0}{2\omega}\frac{e}{m}\right)^2\left|\int_0^t \frac{1}{\Omega}\int d\boldsymbol{r}\left[u^*_{c,k_c}e^{i(\boldsymbol{q}-\boldsymbol{k_c}).\boldsymbol{r}}\{\hat{\mathrm{e}}.\boldsymbol{p}\}u_{v,k_v}e^{+i\boldsymbol{k_v}.\boldsymbol{r}}\right]dt' e^{i(\omega_{cv}-\omega t')}\right. \qquad (2.2.1.12)$$
$$\left. -\int_0^t \frac{1}{\Omega}\int d\boldsymbol{r}\left[u^*_{c,k_c}e^{-i(\boldsymbol{q}+\boldsymbol{k_c}).\boldsymbol{r}}\{\hat{\mathrm{e}}.\boldsymbol{p}\}u_{v,k_v}e^{+i\boldsymbol{k_v}.\boldsymbol{r}}\right] dt'\, e^{i(\omega_{cv}+\omega t')}\right|^2$$

To have a better understanding let us reorder the matrix elements in (2.2.1.12) in the following way. We arrange in the first integral the argument in $\boldsymbol{r}$, that is $\int d\boldsymbol{r}\, u^*_{c,k_c}e^{i(\boldsymbol{q}-\boldsymbol{k_c})\cdot\boldsymbol{r}}\{\hat{\mathrm{e}}\cdot\boldsymbol{p}\}u_{v,k_v}e^{i\boldsymbol{k_v}\cdot\boldsymbol{r}}$. The $\boldsymbol{p}$ operator acts only on terms of the right site i.e. $\boldsymbol{p}\left(u_{v,k_v}e^{i(\boldsymbol{k_v})\cdot\boldsymbol{r}}\right) = e^{i(\boldsymbol{k_v}.\boldsymbol{r})}\boldsymbol{p}\,u_{v,k_v} + \hbar\, k_v u_{v,k_v}\, e^{i(\boldsymbol{k_v}.\boldsymbol{r})}$. Applying this in (2.2.1.12) and taking into account the orthogonally of the Bloch states we see that the second term of the expansion of $\boldsymbol{p}\left(u_{v,k_v}e^{i(\boldsymbol{k_v})\cdot\boldsymbol{r}}\right)$ does not contribute.

$$P_{cv} = \left(\frac{E_0}{2\omega}\frac{e}{m}\right)^2\left|\int_0^t \frac{1}{\Omega}\int d\boldsymbol{r}\left[u^*_{c,k_c}e^{i(\boldsymbol{q}-\boldsymbol{k_c}+\boldsymbol{k_v}).\boldsymbol{r}}\{\hat{\mathrm{e}}.\boldsymbol{p}\}u_{v,k_v}\right]dt' e^{i(\omega_{cv}-\omega t')}\right. \qquad (2.2.1.13)$$
$$\left. -\int_0^t \frac{1}{\Omega}\int d\boldsymbol{r}\left[u^*_{c,k_c}e^{-i(\boldsymbol{q}+\boldsymbol{k_c}-\boldsymbol{k_v}).\boldsymbol{r}}\{\hat{\mathrm{e}}.\boldsymbol{p}\}u_{v,k_v}\right] dt'\, e^{i(\omega_{cv}+\omega t')}\right|^2$$

Where $\omega_{cv} = \omega_c - \omega_v$ is the Bohr frequency. We can split the *r*-integration in two parts by replacing $\boldsymbol{r} = \boldsymbol{R_j} + \boldsymbol{r'}$ where $\boldsymbol{r}'$ lies within a unit cell and $\boldsymbol{R_j}$ is a lattice vector.

Because of the periodicity of the functions u_{c,k_c} and u_{v,k_v} we find the following expression (2.2.1.14) for the first integral in $\boldsymbol{r}$ [9].

$$\frac{1}{\Omega}\int d\boldsymbol{r}\left[u^*_{c,k_c}e^{i(\boldsymbol{q}-\boldsymbol{k_c}+\boldsymbol{k_v}).\boldsymbol{r}}\{\hat{e}.\boldsymbol{p}\}u_{v,k_v}\right] = \left(\sum_j e^{i(\boldsymbol{q}-\boldsymbol{k_c}+\boldsymbol{k_v}).\boldsymbol{R_j}}\right)\frac{1}{\Omega}\int_\Omega d\boldsymbol{r'}\left[u^*_{c,k_c}e^{i(\boldsymbol{q}-\boldsymbol{k_c}+\boldsymbol{k_v}).\boldsymbol{r'}}\{\hat{e}.\boldsymbol{p}\}u_{v,k_v}\right] \quad (2.2.1.14)$$

The summation in equation (2.2.1.14) is the integral representation of the Kronecker Delta which ensures the momentum conservation. This can be done for both integrals in $\boldsymbol{r}$ of the equation (2.2.1.13). To reduce the terms further it is convenient to make the following definition: $M_{cv} := \frac{1}{\Omega}\int_\Omega d\boldsymbol{r}\left[u^*_{c,k_c}e^{i(\boldsymbol{q}-\boldsymbol{k_c}+\boldsymbol{k_v}).\boldsymbol{r'}}\{\hat{e}.\boldsymbol{p}\}u_{v,k_v}\right]$ and $M'_{cv} := \frac{1}{\Omega}\int_\Omega d\boldsymbol{r}\left[u^*_{c,k_c}e^{-i(\boldsymbol{q}+\boldsymbol{k_c}-\boldsymbol{k_v}).\boldsymbol{r'}}\{\hat{e}.\boldsymbol{p}\}u_{v,k_v}\right]$ and then we can rewrite the equation (2.2.1.13) in a reduced form shown in equation (2.2.1.15):

$$P_{cv} = \left(\frac{E_0}{2\omega}\frac{e}{m}\right)^2\left|\delta_{q+k_v,k_c}M_{cv}\int_0^t dt' e^{i(\omega_{cv}-\omega t')} - \delta_{q+k_c,k_v}M'_{cv}\int_0^t dt' e^{i(\omega_{cv}+\omega t')}\right|^2 \quad (2.2.1.15)$$

We will later show that $\delta_{q+k_v,k_c}M_{cv}$ and $\delta_{q+k_c,k_v}M'_{cv}$ are actually equal terms after a proper approximation. Now let us concentrate in the time integral and later we will come back to the *r*-integration. The integrals $\int_0^t dt' e^{i(\omega_{cv}\pm\omega t')}$ can be solved explicitly, see the equation (2.2.1.16),

$$\left|\int_0^t dt' e^{i(\omega_{cv}\pm\omega t')}\right|^2 = \left|\frac{e^{i(\omega_{cv}\pm\omega)t}-1}{i(\omega_{cv}\pm\omega)}\right|^2 \quad (2.2.1.16)$$

The expression with the plus sign, the so called resonance term is attributed to the absorption process where an electron is excited from the valence band to the conduction band and a photon with energy $\hbar\omega$ is absorbed. The second term with the minus sign is called anti-resonance due to the fact that when $\omega = -\omega_{cv}$ we have a singularity too. This is attributed to the stimulated emission where an excited electron in the conduction

band falls into the valence band by emitting a photon with energy $\hbar\omega$ induced by a photon with the same energy. The Bohr frequency is related to the necessary energy to excite an electron between the bands. Because we want to describe the fundamental absorption of solids, the last process of stimulated emission will not be taken into account for the absorption coefficient in crystalline solids at zero Kelvin temperature due to the fact that at this temperature all the electrons are in the valence state.

To solve the equation (2.2.1.16) we can use the following relations (2.2.1.17) and (2.2.1.18), taking into account that the elapsed time is large enough.

$$\left|1 - e^{i\theta}\right|^2 = 4\,\mathrm{sen}^2\left(\frac{\theta t}{2}\right) \tag{2.2.1.17}$$

$$\lim_{t\to\infty} \frac{1}{t}\left(\frac{\mathrm{sen}^2(xt/2)}{x^2}\right) = \frac{\pi}{2}\delta(x) \tag{2.2.1.18}$$

Using these relations into equation (2.2.1.16) we find the equation (2.2.1.20) where we have defined $E_{cv} = \hbar\omega_{cv}$.

$$\left|\int_0^t dt'\, e^{i(\omega_{cv} \pm \omega t')}\right|^2 = \frac{2\pi t}{\hbar}\delta(E_{cv} \pm E) \tag{2.2.1.20}$$

The result of equation (2.2.1.20) is obviously related to the energy conservation in the respective process of absorption and stimulated emission. And it let us write the equation (2.2.1.15) of the probability in a more compact form (see equation 2.2.1.21). The momentum conservation corresponds to the absorption as $k_c = q + k_v$ and for the stimulated emission as $k_v = q + k_c$. This can easily be seen in equation (2.2.1.21) where we make the summation through all possible wave vectors $\boldsymbol{k}$, because all processes with any $\boldsymbol{k_c}$ and $\boldsymbol{k_v}$ contribute to the total probability P_{cv} for a transition between the valence band and conduction band.

$$P_{cv} = \frac{2\pi t}{\hbar}\left(\frac{E_0}{2\omega}\frac{e}{m}\right)^2 \sum_{k_c,k_v} \left[\left|M_{cv}\right|^2 \delta(E_{cv} - E)\delta_{q+k_v,k_c} - \left|M'_{cv}\right|^2 \delta(E_{cv} + E)\delta_{q+k_c,k_v}\right] \tag{2.2.1.21}$$

At this point it is convenient to make the following approximation. The effect of the photon momentum $\boldsymbol{q}$ in the transitions can be neglected always as we work with visible light. To apply this on the matrix elements let us first take into account the momentum conservation for each process. The exponential term in the matrix elements M_{cv} and M'_{cv} becomes the value one and the functions u_{c,k_c} and u_{v,k_v} are therefore related by the photon momentum.

$$M_{cv} = \int d\boldsymbol{r}\, u^*_{c,k_v+q}\{\hat{e}.\boldsymbol{p}\}u_{v,k_v}$$
$$M'_{cv} = \int d\boldsymbol{r}\, u^*_{c,k_c}\{\hat{e}.\boldsymbol{p}\}u_{v,k_c+q} \qquad (2.2.1.22)$$

For a small photon momentum $\boldsymbol{q}$, the functions u_{c,k_v+q} and u_{v,k_c+q} can be expanded in Taylor series [9].

$$u_{c,k_v+q} = u_{c,k_v} + \boldsymbol{q}.\nabla u_{c,k_v} + \ldots \approx u_{c,k_v}$$
$$u_{v,k_c+q} = u_{v,k_c} + \boldsymbol{q}.\nabla u_{v,k_c} + \ldots \approx u_{v,k_c} \qquad (2.2.1.23)$$

By neglecting the photon momentum, using the equations (2.2.1.22) and (2.2.1.23) the matrix elements M_{cv} and M'_{cv} become identical. See equation (2.2.1.24), where we renamed $\boldsymbol{k} = \boldsymbol{k}_c = \boldsymbol{k}_v$.

$$M_{cv} = M'_{cv} = \int d\boldsymbol{r}\, u^*_{c,k}\{\hat{e}.\boldsymbol{p}\}u_{v,k} \qquad (2.2.1.24)$$

Finally, the probability P_{cv} has its final form shown in equation (2.2.1.25).

$$P_{cv} = \frac{2\pi t}{\hbar}\left(\frac{E_0 e}{2\omega m}\right)^2 \sum_{k_c,k_v} |M_{cv}|^2\{\delta(E_{cv} - \hbar\omega) - \delta(E_{cv} + \hbar\omega)\}\,\delta_{k_v,k_c} \qquad (2.2.1.25)$$

The transition rate per volume unit R_{cv} as it was mentioned at the beginning of this section is defined by the transition probability by $R_{cv} = dP_{cv}/dt$ (see equation 2.2.1.26).

$$R_{cv} = \frac{2\pi}{\hbar}\left(\frac{E_0 e}{2\omega m}\right)^2 \sum_{k_c,k_v} |M_{cv}|^2 \{\delta(E_{cv} - \hbar\omega) - \delta(E_{cv} + \hbar\omega)\}\delta_{k_v,k_c} \qquad (2.2.1.26)$$

The equation (2.2.1.26) it is known as Fermi's Golden Rule, in this case for Bloch electrons with transitions between the valence and conduction bands in a crystal. From the equation (2.2.1.6) and (2.2.1.26) we can obtain the absorption coefficient. We consider only the absorption term and not the stimulated emission term (see equation 2.2.1.27).

$$\alpha = \frac{\hbar}{4\pi\epsilon_0 nc}\left(\frac{2\pi e}{m}\right)^2 \frac{1}{\hbar\omega} \sum_{k_c,k_v} |M_{cv}|^2 \delta(E_c - E_v - \hbar\omega)\, \delta_{k_v,k_c} \qquad (2.2.1.27)$$

The equation (2.2.1.27) matches the equation (8.9) in the reference [12] (chapter 8, page 139). The summation over the vector $\boldsymbol{k}$ of equation (2.2.1.27) can be written as a summation over the energy due to the relation between the energy bands and the vector $\boldsymbol{k}$ when we use the free electron approximation. These summations can be calculated by using the density of electronic states (see equation 2.2.1.28).

$$\sum_k = \sum_E \rightarrow \int D(E)dE \qquad (2.2.1.28)$$

The density of electronic states can be calculated by several ways, one of them used in reference [9] is shown in equation (2.2.1.29), where dS_k is the surface differential element in the $\boldsymbol{k}$ space, $\nabla_k E$ is the gradient in $\boldsymbol{k}$ of the energy $E(k)$, and the number two in the equation is because of the spin electron degeneracy.

$$D(E) = \frac{2}{(2\pi)^3} \int \frac{dS_k}{|\nabla_k E|} \qquad (2.2.1.29)$$

Our goal is now to reduce the equation (2.2.1.27) in a simple analytical expression that depends on the photon energy which we are able to fit with a measured absorption coefficient by optical means. For this, let us expand the band energies E_c and E_v around

$\boldsymbol{k} = \mathbf{0}$ till the second order term assuming for simplicity that the effective mass is uniform in the $\boldsymbol{k}$ space, see the equations (2.2.1.30).

$$\begin{aligned} E_c &= E_c(0) + \frac{\hbar}{2m_e^*}k^2 \ \ldots \\ E_v &= E_v(0) - \frac{\hbar}{2m_h^*}k^2 \ldots \end{aligned} \tag{2.2.1.30}$$

Choosing the energy reference frame in a way that $E_c(0) = E_g$ and $E_v(0) = 0$, with E_g the optical bandgap, we can define the energy band of combined states according to the equation (2.2.1.31), where we introduce the reduced mass $\mu^{-1} = m^{*}_{e}{}^{-1} + m^{*}_{h}{}^{-1}$ [9].

$$E_{cv} \equiv E_c - E_v = E_g + \frac{\hbar}{2\mu}k^2 \tag{2.2.1.31}$$

It is important to remark that the definition of the energy band of combined states E_{cv} only has sense in direct solids, because the functions E_c and E_v share the same vector $\boldsymbol{k}$ as their argument for direct transitions. Now, from the equations (2.2.1.31) and (2.2.1.29) we find the electronic density of combined states (see equation 2.2.1.32).

$$D_{cv} = \sqrt{2}\frac{\mu^{3/2}}{\pi^2\hbar^3}\left(E_{cv} - E_g\right)^{1/2} \quad , \quad \mathrm{E_{cv}} > \mathrm{E_g} \tag{2.2.1.32}$$

Finally, from equations (2.2.1.32), (2.2.1.28), (2.2.1.27), assuming that the matrix element M_{cv} changes slowly with $\boldsymbol{k}$ [6][9] and solving the trivial integral we find an analytical expression for the absorption coefficient as a function of the photon energy $\hbar\omega$ and the optical bandgap E_g shown in equation (2.2.1.33).

$$\alpha = \frac{\sqrt{2}\mu^{3/2}}{4\pi\epsilon_0\, nc\, \hbar^2}\left(\frac{2e}{m_e}\right)^2 |M_{cv}|^2 \frac{\left(\hbar\omega - E_g\right)^{1/2}}{\hbar\omega} \tag{2.2.1.33}$$

The obtained result in equation (2.2.1.33) is known as the fundamental absorption of direct semiconductors (i.e. *c*-AlN), due to the fact that only direct transitions between the valence and conduction bands are considered, that is with the same vector $\boldsymbol{k}$

neglecting the photon momentum $\boldsymbol{q}$, and it contains explicit information of the solid's optical bandgap.

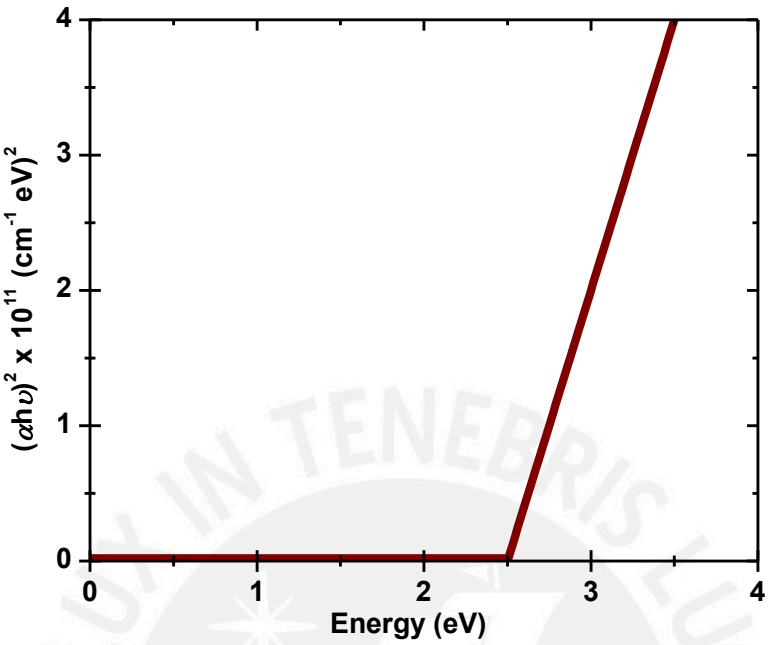

Figure: 2.2.1.1: Representation of the fundamental absorption for an ideal direct semiconductor at zero Kelvin temperature using the equation (2.2.1.33).

A common representation of the absorption coefficient to evaluate the optical bandgap is the $(\alpha hvn)^2$ plot shown in the figure (2.2.1.1) where the linear behavior allows reading directly the bandgap energy. It is important to remark that the refractive index usually varies between 1 and 3 in most of the spectral range and therefore it is usually taken as constant not affecting the energy dependency of the absorption coefficient.

Fundamental absorption in direct crystals at finite temperatures

In the last sub-section we found an analytical expression for the absorption coefficient as a function of the photon energy and the optical bandgap valid only for direct transitions and for a completely filled valence band by electrons and conduction band by holes. However, the behavior described in the last section only has validity when the temperature is zero degree Kelvin. In the reality we deal with temperatures much higher than zero degree Kelvin and therefore the valence and conduction bands do not meet the conditions mentioned above. In this section we will derivate an expression for the absorption coefficient taking into account finite temperatures.

For this it is necessary to consider the term associated to the stimulated emission found in the last section, because for temperatures higher than zero degree Kelvin the valence band is not completely filled and the conduction band is not completely free of electrons. Therefore the few electrons in the conduction band will fall into the valence band due to the stimulated emission and this effect should be taken into account.

$$R_{cv} = \frac{2\pi}{\hbar}\left(\frac{E_0 e}{2\omega m}\right)^2 \sum_{k_c,k_v} |M_{cv}|^2 \{\delta(E_{cv} - \hbar\omega) - \delta(E_{cv} + \hbar\omega)\}\delta_{k_v,k_c} \qquad (2.2.2.1)$$

We will start from the equation (2.2.1.26) found in the last section here numbered (2.2.2.1). Before we continue it is important to make some remarks. First, the absorption term in the equation (2.2.2.1) represents a transition from the valence band state $|v\rangle$ to the conduction band sate $|c\rangle$ while the stimulated emission term represents a transition from the state $|c\rangle$ to the state $|v\rangle$. Second, the equation (2.2.2.1) gives us the transition rate of one electron, but in real systems we deal with an ensemble of electrons. The Fermi distribution $f(E)$ determines the occupation grade of the electrons for each band; it is shown in equation (2.2.2.2) where $\beta = 1/\kappa T$ with T the temperature, E_f the Fermi level, and κ the Boltzman constant.

$$f(E) = \frac{1}{1 - e^{-\beta(E - E_f)}} \qquad (2.2.2.2)$$

Our goal is to find the mean absorption coefficient by averaging all the initial states taking into account the Pauli's exclusion principle [14][15]. This can be done by using the Fermi distribution properly in each of the two processes, absorption and stimulated emission. Thus we consider all the occupied states by electrons in the valence band by multiplying the density of states of the valence band by $f(E_v)$, and we consider all de unoccupied states by electrons or occupied by holes by multiplying the density of states of the conduction band by $\big(1 - f(E_c)\big)$. As it was suggested in the reference [15] these products can be applied on the equation (2.2.2.1) in the sense that this equation contains the mentioned density of states in its argument when is expressed in its integral form following what was done in the equation (2.2.1.28). The exclusion principle is taken into account by dividing the transition rate by two, (see the equation 2.2.2.3).

$$\langle R_{cv}\rangle = \frac{\pi}{\hbar}\left(\frac{E_0 e}{\omega m}\right)^2 \sum_{k_c,k_v} |M_{cv}|^2 f(E_v)\{\delta(E_c - E_v - \hbar\omega) - \delta(E_c - E_v + \hbar\omega)\}\big(1 - f(E_c)\big)\delta_{k_v,k_c} \tag{2.2.2.3}$$

At this point it is convenient to write the matrix element in the following notation $|M_{cv}| = \langle c|M'_{cv}|v\rangle$ and $C = \pi/\hbar\,(E_0 e/\omega m)^2$. Let us split the equation (2.2.2.3) in two similar terms shown in equation (2.2.2.4).

$$\langle R_{cv}\rangle = C\left(\sum_{k_c,k_v} \left|\langle c|M'_{cv}|v\rangle\right|^2 \{ f(E_v)\delta(E_c - E_v - \hbar\omega)\big(1 - f(E_c)\big)\} - \sum_{k_c,k_v} \left|\langle c|M'_{cv}|v\rangle\right|^2 \{f(E_v)\delta(E_c - E_v + \hbar\omega)\big(1 - f(E_c)\big)\}\right) \tag{2.2.2.4}$$

As we know, the Dirac's delta factors ensure the energy conservation in each process. Following the reference [15] we can effectuate one of the summations by using its integral form i.e. $\sum_{k_c} \to \sum_{E_c} \to 1/\Delta E_c \int dE_c$, thus we get a factor of $1/\Delta E_c$, see the equation (2.2.2.5).

$$\langle R_{cv}\rangle = C\frac{1}{\Delta E_c}\left(\sum_{k_c} \left|\langle v + \hbar\omega|M'_{cv}|v\rangle\right|^2 \{ f(E_v) - f(E_v)f(E_v + \hbar\omega)\} - \sum_{k_c} \left|\langle v - \hbar\omega|M'_{cv}|v\rangle\right|^2 \{f(E_v) - f(E_v)f(E_v - \hbar\omega)\}\right) \tag{2.2.2.5}$$

Let us concentrate on the second term in the equation (2.2.2.5) that corresponds to the stimulated emission. In this term we can rename the initial state in the following way $|v - \hbar\omega\rangle = |v'\rangle$ and therefore the final state by $|v\rangle = |v' + \hbar\omega\rangle$, in terms of the energy $E_c = E_v - \hbar\omega = E_{v'}$. The second term can be written as shown in equation (2.2.2.6) where we have only renamed the variables maintaining the energy conservation valid.

$$-\sum_{k_{v'}}|\langle v'|M'_{cv}|v'+\hbar\omega\rangle|^2\{f(E_{v'}+\hbar\omega)-f(E_{v'})f(E_{v'}+\hbar\omega)\} \qquad (2.2.2.6)$$

The index of the summation in the equation (2.2.2.6) is mute, and thus both summations in the equation (2.2.2.5) are reduced to one, the resulting formula shown in the equation (2.2.2.7) is known as Kubo-Greenwood formula [14][15].

$$\langle R_{cv}\rangle = \frac{C}{\Delta \mathrm{E_c}}\sum_{k_v}|M_{cv}|^2\{f(E_v)-f(E_v+\hbar\omega)\} \qquad (2.2.2.7)$$

However, the equation (2.2.2.7) can be reduced further. We derivate an expression for the absorption coefficient similar to the one found in the previous section starting from the equation (2.2.2.7) to include the temperature dependence. According to reference [15] we rewrite the equation (2.2.2.7) as it is shown in equation (2.2.2.8) where $E=\hbar\omega$ is the photon energy.

$$\langle R_{cv}\rangle = C\sum_{k_c,k_v}|M_{cv}|^2\{f(E_v)-f(E_c)\}\delta(E_c-E_v-E) \qquad (2.2.2.8)$$

From equation (2.2.2.8) we will solve the summation over k_c using the density of states to replace the mentioned summation into an integral as it was done in the last section, that is $\sum_{k_c} = \sum_{E_c} \rightarrow \int D_c(E_c)\,dE_c$, and then we will write the summation over k_v in its integral form. The integral in E_c is trivial and absorbing the constants into the coefficient C we get the form shown in the equation (2.2.2.9).

$$\langle R_{cv}\rangle = C\sum_{k_v}|M_{cv}|^2\sqrt{E_v+E-E_g}\,\{f(E_v)-f(E_v+E)\} \qquad (2.2.2.9)$$

As it was mentioned above, the summation in the equation (2.2.2.9) can be replaced by its integral form, that is $\sum_{k_v} = \sum_{E_v} = \lim_{\Delta E_v\to 0} \frac{1}{\Delta E_v}\int dE_v$. Rewriting the equation (2.2.2.9) into its integral form (see equation 2.2.2.10) it is possible to note the definition of the derivative of the Fermi distribution with $\Delta E_v \equiv \hbar\omega$ the change in energy, properly as the photon energy, this is easily seen as the difference in energy between the

bands or states $|v\rangle$ and $|c\rangle$, that is $E = E_c - E_v$ the photon energy. Thus we can write the definition of the derivative as shown in the equation (2.2.2.11).

$$\langle R_{cv} \rangle = C \int_{E_g - E}^{E_g} |M_{cv}|^2 \sqrt{E_v + E - E_g} \left(\lim_{\Delta E_v \to 0} \frac{f(E_v) - f(E_v + E)}{\Delta E_v} \right) dE_v \qquad (2.2.2.10)$$

$$\frac{df(E_v)}{dE_v} = \lim_{\Delta E_v \to 0} \frac{f(E_v + E) - f(E_v)}{\Delta E_v} \qquad (2.2.2.11)$$

Finally using the equations (2.2.2.10) and (2.2.2.11) we find an expression for the average transition rate between bands shown in the equation (2.2.2.12). This equation unfortunately has no analytical solution. The average absorption coefficient follows to be related to the average transition rate along with the equation (2.2.1.6). The integral limits in the equation (2.2.2.12) are $E_g - E$ for the lower limit and E_g for the upper limit.

$$\langle R_{cv} \rangle = C \int_{E_g - E}^{E_g} |M_{cv}|^2 \sqrt{E_v + E - E_g} \left(-\frac{df(E_v)}{dE_v} \right) dE_v \qquad (2.2.2.12)$$

It is also possible to write the equation (2.2.2.12) in an equivalent form, see the equation (2.2.2.13) but with a more familiar shape by adding E to the integral limits and therefore subtracting E from the integral's argument and renaming the mute variable E_v by E_{cv}.

$$\langle R_{cv} \rangle = C \int_{E_g}^{E_g + E} |M_{cv}|^2 \sqrt{E_{cv} - E_g} \left(-\frac{df(E_{cv} - E)}{dE_{cv}} \right) dE_{cv} \qquad (2.2.2.13)$$

The equations (2.2.2.12) and (2.2.2.13) are equivalent but the second has a similar form to the result found in the last section, except that instead of a Dirac's delta we have minus the derivative of the Fermi distribution with the argument $(E_{cv} - E)$. The derivative of the Fermi function in the limit case of $T = 0$ behaves like a Dirac's delta around the Fermi level E_f. The discontinuities of the shape of the Fermi distribution at

$T = 0$ and its derivative are smeared out for temperatures larger than zero (see fig. 2.2.2.1). Thus for direct transitions at a finite temperature it is enough to replace the Dirac's delta function associated to the energy conservation by minus the derivative of the Fermi distribution evaluated in the same argument.

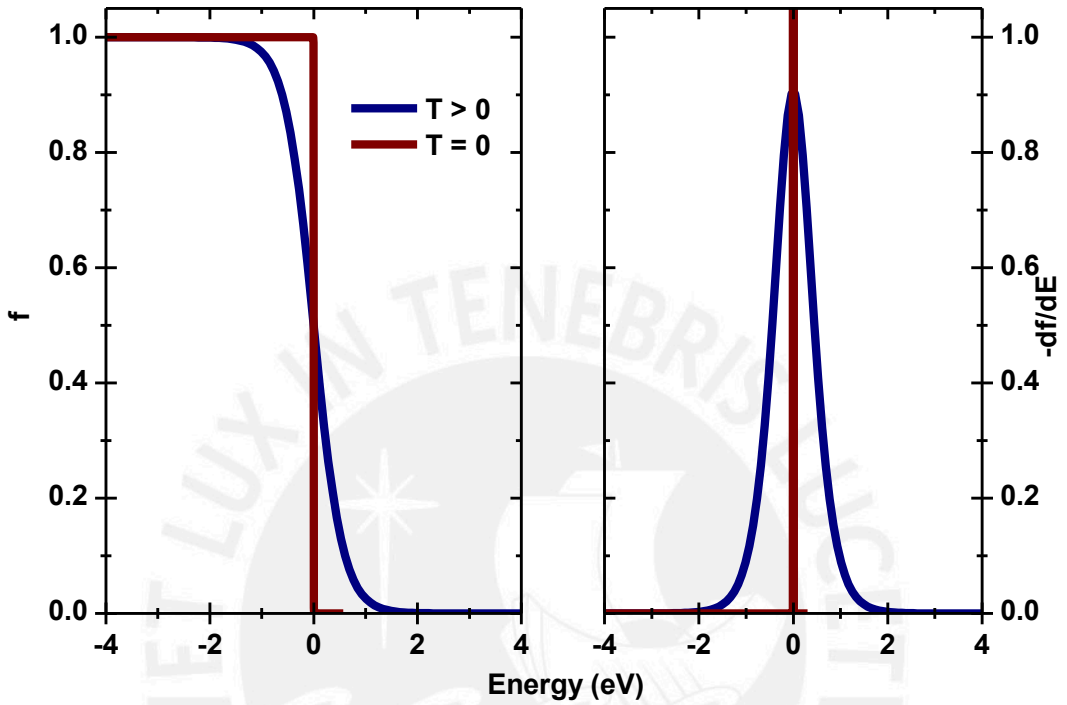

Fig. 2.2.2.1: Fermi distribution (left) and minus the derivative of the Fermi distribution (right) versus the energy in the cases of zero Kelvin temperature and for a higher temperature. In this graphs the Fermi energy was taken as zero.

Finally the absorption coefficient can be calculated, see the equation (2.2.2.14), leaving all the constants in the coefficient C. The integral in these equations has no analytical solution but it can be solved by numerical methods.

$$\langle \alpha \rangle = \frac{C}{E} \int_{E_g}^{E_g + E} \sqrt{E_{cv} - E_g} \left(- \frac{df(E_{cv} - E)}{dE_{cv}} \right) dE_{cv} \qquad (2.2.2.14)$$

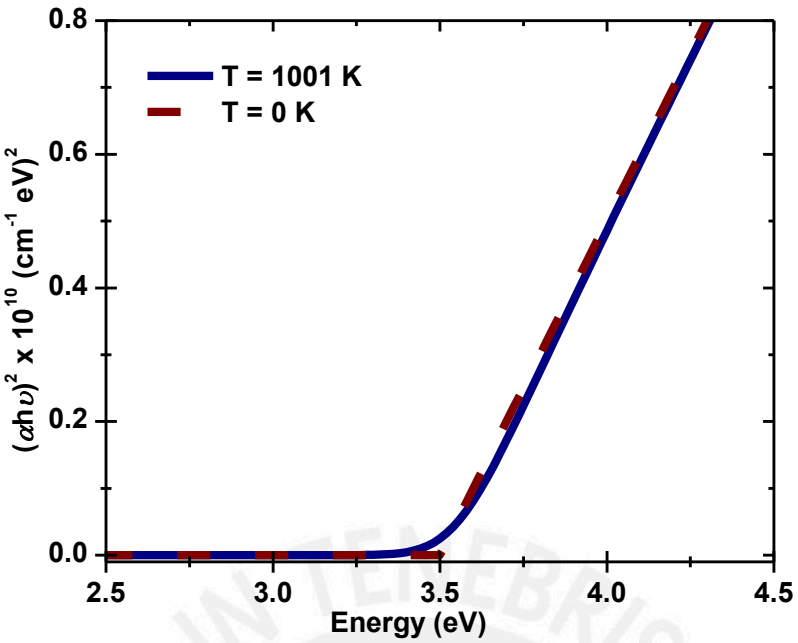

Figure 2.2.2.2: Fundamental absorption for an ideal direct semiconductor at zero Kelvin temperature (dashed red curve) and at a finite temperature (continue blue curve). The simulation was made using the equations (2.2.1.31) and (2.2.2.14) with a zero Fermi energy.

If we plot the function $(\alpha E)^2$ for both cases at zero Kelvin temperature and for a higher temperature we will be able to observe (see fig. 2.2.2.2) the formation of a tail due to the thermal vibrations or thermal disorder in the lattice crystal. One is able to see the characteristic line that allows us to find the optical bandgap by the intersection of its prolongation to the *x*-axis. From the comparison shown in the figure (2.2.2.2) and the comparison of the equations (2.2.2.14) and (2.2.1.33) we can say that the integral term of the equation (2.2.2.14) is similar to the term $\left(\hbar\omega - E_g\right)^{1/2}$ of the equation (2.2.1.33). Therefore it is possible to consider this term as from an effective electronic density of combined states (see figure 2.2.2.3).

In this sense, the tail of states below the bandgap is the result of the extra energy the electrons gain from the thermal vibrations or absorbing phonons. The reduction of states over the bandgap region is the result of the energy loss due to the same thermal vibrations or emitting phonons.

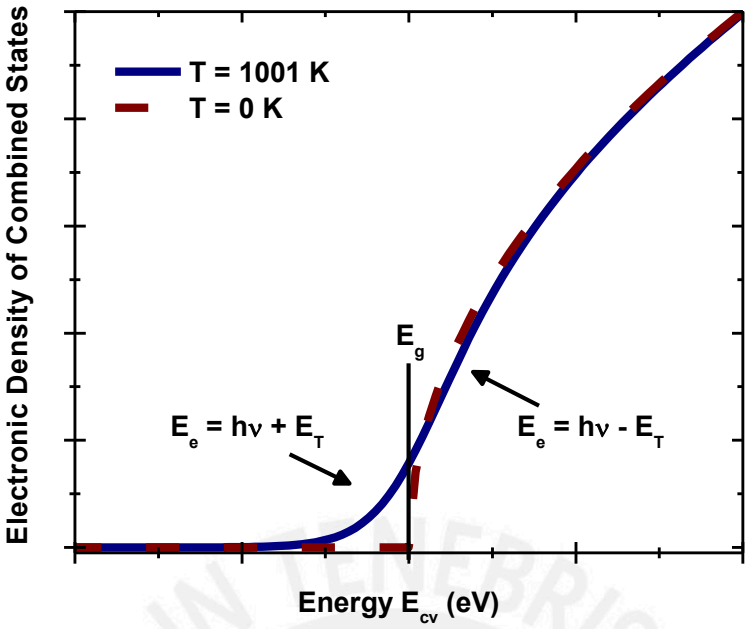

Figure 2.2.2.3: Schematic representation of the electronic density of combined states at zero Kelvin temperature and the effective electronic density of combined states for a higher temperature in a crystal lattice. E_e is the electron energy, $h\nu$ the photon energy, E_T the thermal energy.

Summarizing, there is a tail of states below the bandgap due to the thermal disorder, the main transitions are between the valence and conduction band sates and therefore the optical bandgap is maintained. These states can be represented in an effective electronic density of combined states shown in the figure (2.2.2.3), where E_g is the bandgap.

Fundamental absorption in amorphous solids

In the amorphous case, the absorption coefficient calculation can be developed in the same way as in the crystalline case. However, it is not possible to define an energy band of combined states like before because the vector $\boldsymbol{k}$ is not a good quantum number in the amorphous case [6][11][12]. It is always possible to define quasi-continuum states that are called extended states [6]. Besides of these extended states there exist the so called tail states (see fig. 2.2.3.1) similar to the states found due to the thermal vibrations in the last section. These localized states are mainly caused by the lattice disorder of the amorphous solid, defects, dangling bonds and as it was shown in the last section by thermal vibrations.

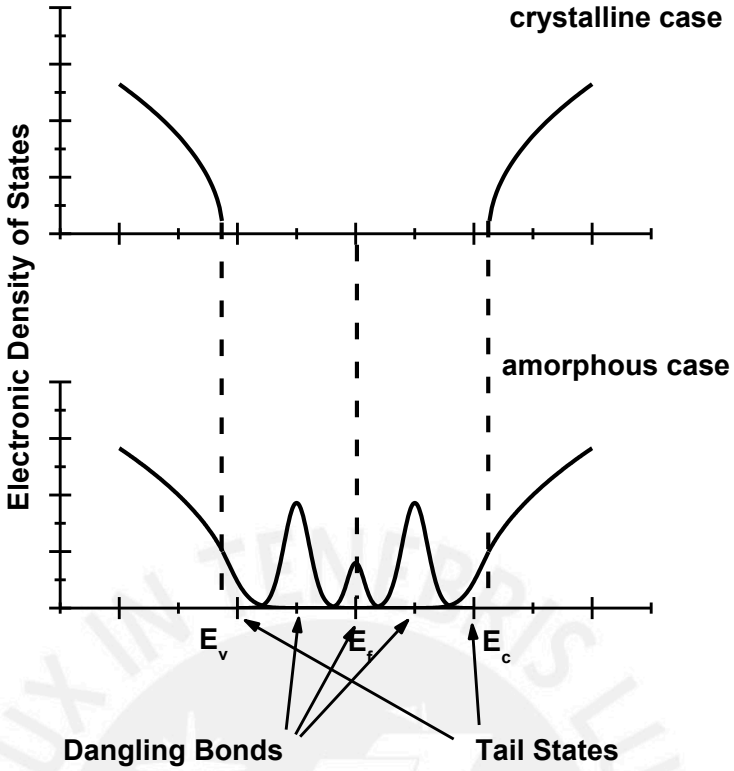

Figure 2.2.3.1: Representation of the electronic density of states for the crystalline and amorphous cases. Notice that the valence and conduction band edges in the amorphous case are inside of the band tails or Urbach tails. The states inside the gap are due to the dangling bonds.

So far we haven't defined properly what amorphousness or disorder is, therefore before we continue into the fundamental absorption in amorphous materials let us clarify this issue. Disorder must be compared to a standard. In this case the standard is a perfect crystal. A perfect crystal is that in which the atoms are arranged in a pattern that repeats periodically to an infinite extent [9][11][12][16]. From this point, we will define three main types of disorder. The first one is the topological or geometrical disorder where the atoms are arranged completely randomly and there is no translational periodicity (see fig. 2.2.3.2.a). All amorphous solids are distinguished by their lack of periodicity; however, certain amorphous materials have considerable short-range or local order while others have little, but both cases have no long-range order. The second kind of disorder is the substitutional disorder. I. e. in alloys where while the crystalline lattice is preserve the compound has one type of atom substituting randomly for the other in the lattice (see fig. 2.2.3.2.b). The third type of disorder of interest is the vibrational disorder of a crystalline lattice, this starts from the concept of perfect crystal that is only

possible at zero Kelvin temperature, and for a finite temperature the motion of atoms around their equilibrium positions ruins the perfect periodicity (see fig. 2.2.3.2(c)).

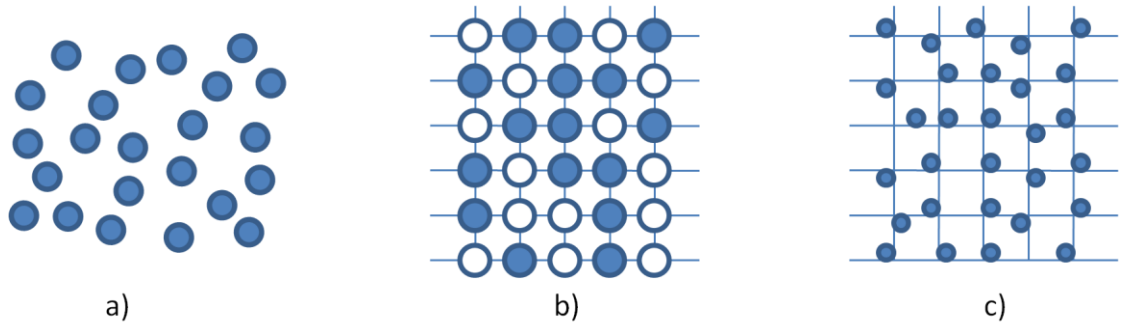

Figure 2.2.3.2: Representation of the types of randomness or disorder in solids. a) topological disorder, the atoms are completely randomly arranged in the space, b) substitutional disorder, the atoms in the compound are randomly arranged on the crystalline lattice c) vibrational disorder, the atoms vibrate about their equilibrium crystalline positions.

It is possible to define disorder energy or fictive temperature that represents the disorder degree. This disorder energy would be closely related to the tail in the absorption coefficient. This topic will be treated in detail in the chapter four.

In principle in amorphous solids we have transitions of the type extended-extended, localized-localized and extended-localized [12][17]. To determine the shape of these states have been and is yet a difficult problem [18-20], thus it have been only possible to give empirical representations of them to determine the optical bandgap trough the measure of the absorption coefficient [7][18][19]. The simplest case is the transitions between extended sates or extended-extended type transitions. This was developed by J. Tauc (1968) [7]. We will continue in this section developing the approach made by J. Tauc for transitions between the conduction and valence extended states assuming a quadratic form for their energy bands.

The extended to extended transitions can be develop in the same way as in the crystalline after assuming a shape for the energy bands or for the density of states. The absorption coefficient can then be written as the equation (2.2.3.1).

$$\alpha = \frac{\hbar}{4\pi\epsilon_0 nc}\left(\frac{2\pi e}{m}\right)^2 \frac{1}{\hbar\omega}\sum_{E_c,E_v} |M_{cv}|^2 \delta(E_c - E_v - \hbar\omega) \qquad (2.2.3.1)$$

From the equation (2.2.3.1) the formulation for the crystalline case can be completely adopted and the double summation becomes a double integral using the density of electronic states and assuming again that the matrix element M_{cv} changes slowly with the energy and therefore it is assumed constant. The equation (2.2.3.1) can be written as shown in the equation (2.2.3.2) where all the constants have been putted in the coefficient C.

$$\alpha = \frac{C}{E}\int_{E_g}^{E_c-E_v}\int_{E_g-E}^{0} D_c(E_c)D_v(E_v)\delta(E_c - E_v - E)dE_v dE_c \qquad (2.2.3.2)$$

Assuming a quadratic form for the energy bands (see equation 2.2.1.30) it follows from the equation (2.2.1.29) that the electronic density of states has a square root dependency, $D_c = (\sqrt{2}m^{*3/2}_e/\pi^2\hbar^3)(E_c - E_g)^{1/2}$ and $D_c = (\sqrt{2}m^{*3/2}_h/\pi^2\hbar^3)$. Thus the equation (2.2.3.2) is an analytical integral by making the variable change of $x = (E_c - E_g)/(E - E_g)$ the integral's argument changes in a tabulated one which value is a constant and is absorbed in the coefficient C, see the equations (2.2.3.3) and (2.2.3.4). The resulting absorption coefficient shown in equation (2.2.3.4) is the result of J. Tauc, and the optical bandgap obtained from it is known as Tauc-gap E_{Tauc}. The chosen density of states is not the best one to describe every amorphous solid. But it is well known and used in the materials science scientific community.

$$\alpha = \frac{C}{E}(E - E_g)^2\int_0^1 x^{1/2}(1-x)^{1/2}\,dx \qquad (2.2.3.3)$$

$$\alpha = C\frac{(E - E_g)^2}{E} \qquad (2.2.3.4)$$

The main problem with the result (2.2.3.4) is obviously that it has only been taken into account the extended-extended type transitions and it follows that these transitions not always are the predominant ones and thus the relation (2.2.3.4) is not sufficient to describe the fundamental absorption in amorphous solids. Also the fact of assuming a square rooted shape of the density of states can result in mistakes when calculating the bandgap. However, in the literature different exponents are used for describing the

density of states and therefore the fundamental absorption [2][17] in amorphous solids, arguing that the experimental data fits better with the theoretical curve [21] [22]. The truth is that there is no convincing argument for the election of an exponent or a particular shape for the fundamental absorption in amorphous solids, in general this depends on the data and therefore (2.2.3.5) is a phenomenological ansatz [6][12][23].

$$\alpha = \frac{C}{E}\int_{E_g}^{E}\left(E_c - E_g\right)^r (E_c - E)^r dE_c \qquad (2.2.3.5)$$

A way to generalize the result of equation (2.2.3.4) might be through the generalization of the shape of the density of states used in the equation (2.2.3.3). Thus if we leave the exponents as variables we can rewrite the equation (2.2.3.3) as the equation (2.2.3.5) and by making the variable change of $x = \left(E_c - E_g\right)^r/(E - E_c)^r$ we obtain the integral shown in the equation (2.2.3.6).

$$\alpha = C\frac{\left(E - E_g\right)^{2\,r\,+\,1}}{E}\int_0^1 x^r(1-x)^r dx \qquad (2.2.3.6)$$

By solving the integral in equation (2.2.3.6) we find the equation (2.2.3.7) with the gamma function $\Gamma(n)$, where r are natural numbers and therefore the exponent can only have the odd numbers values. Nevertheless, according to the reference [12] for any representation of the absorption coefficient, the coefficient C is a measure of the disorder in the way that for more disordered systems the slope is gentle and for less disordered systems it is higher. This approach of a measure of the disorder by the slope $C^{1/2}$ comes from the idea that for more disordered systems the tail is bigger and therefore it overlaps over the rest of the absorption coefficient making the slope gentler and for less disordered systems the tail is smaller an therefore the slope is higher.

$$\alpha = C\frac{\left(E - E_g\right)^{2\,r\,+\,1}}{E}\frac{\Gamma^2(r+1)}{\Gamma(2r+2)} \qquad (2.2.3.7)$$

It is well known that by annealing treatments on amorphous semiconductors the tail states are reduced and therefore a reduction in the disorder is expected (see fig.

2.2.3.3.a). Effectively the tail is reduced in the case shown in the figure (2.2.3.3.a) but the slope does not change as suggested by reference [12], (see figures 2.2.3.3.c and 2.2.3.3.d) where the two common representations are used. This disagreement might be attributed to the fact that when we compare the absorption coefficient of the *a*-AlN with *c*-AlN we see that for the case shown in the figure (2.2.3.3) we are still far from the fundamental absorption. That is for example assuming the right representation for the fundamental absorption as $(\alpha E)^2$ after 900 °C of annealing treatment (see fig. 2.2.3.3.d) no slope is possible to observe. Results concerning measurements of the absorption coefficient of *a*-AlN are shown in the last chapter showing the proper behavior in agreement with reference [12].

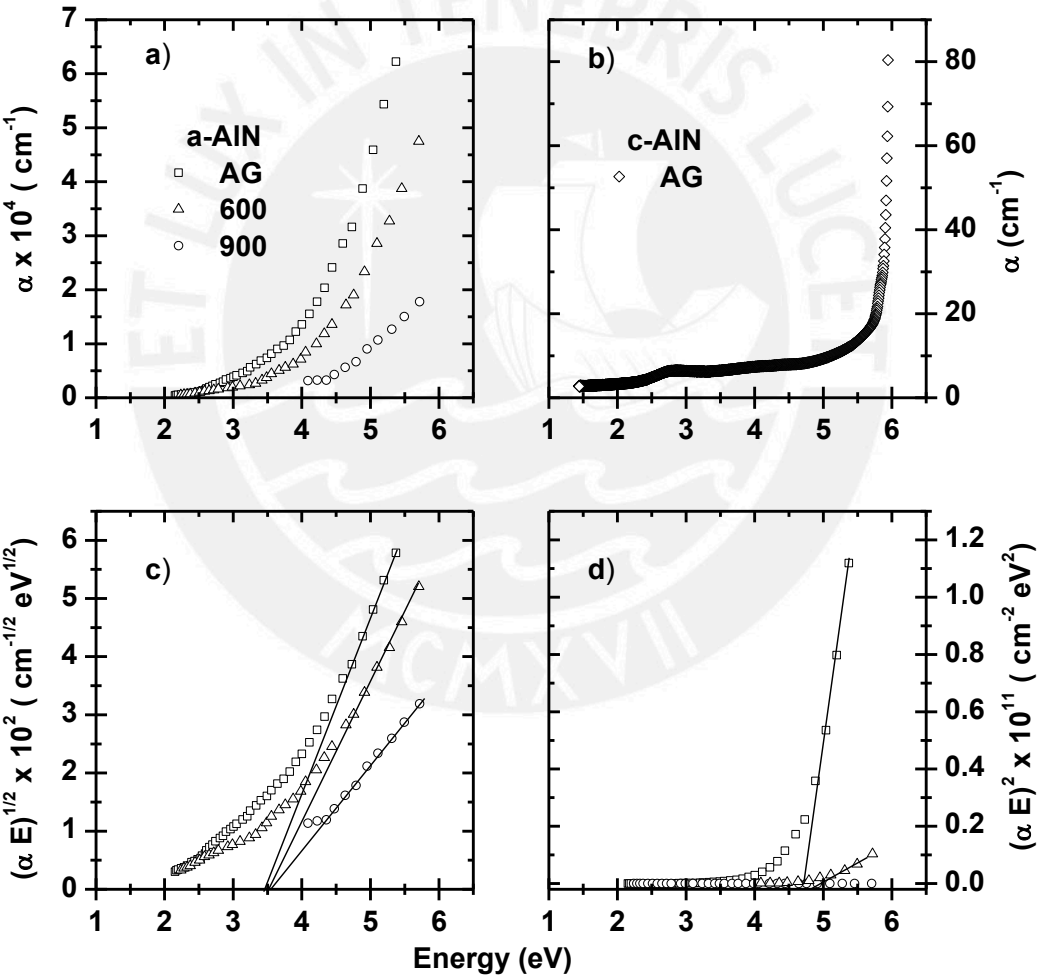

Figure 2.2.3.3: a) Absorption coefficient of *a*-AlN thin film produced by RF-reactive sputtering using an Aluminum target in an atmosphere of Nitrogen [17], b) Absorption coefficient of *c*-AlN (Matthias Bickerman from the group of AlN WW6, Technische Fakultät of Erlangen-Nürnebrg University), c) Tauc-representation of the absorption coefficient of *a*-AlN, d) $(\alpha E)^2$-representation, of the absorption coefficient of *a*-AlN.

Summarizing, we have found plenty of difficulties in the calculation of the fundamental absorption in the amorphous semiconductors. To describe the fundamental absorption we can always use an empirical representation that fits better the measurements. To describe the degree of randomness in an amorphous solid is better to treat it directly with the exponential tail. Nevertheless, the Tauc-representation is the most common used representation for determining the optical bandgap, and therefore we will take it into account in the next chapters of this thesis.

Chapter III

Experimental details

This chapter describes details of the experiments. That is the sample preparation, composition measurements, the annealing treatment and the transmission spectrum measurements.

Sample preparation

The a-$(SiC)_{1-x}(AlN)_x$ thin films were deposited on CaF_2, MgO, Al_2O_3 and glass substrates, by rf dual magnetron sputtering using AlN and SiC wafers (Ø 51mm) of high purity as targets. A schematic figure of the magnetron can be seen in figure (3.1.1). The two targets were mounted below the substrate holder which was cooled at 10°C with a water cooling system to enforce the films in the amorphous state. The sputtering process took place in an argon atmosphere of purity 5N at 8×10^{-3} mbar and argon flow rates of 50 sccm. Each target could be adjusted in position and power independently. Typical rf powers were between 85 W and 140 W. Further details of our sample preparation can be found in [24][25]. The system configuration is shown in the figure (3.1.2).

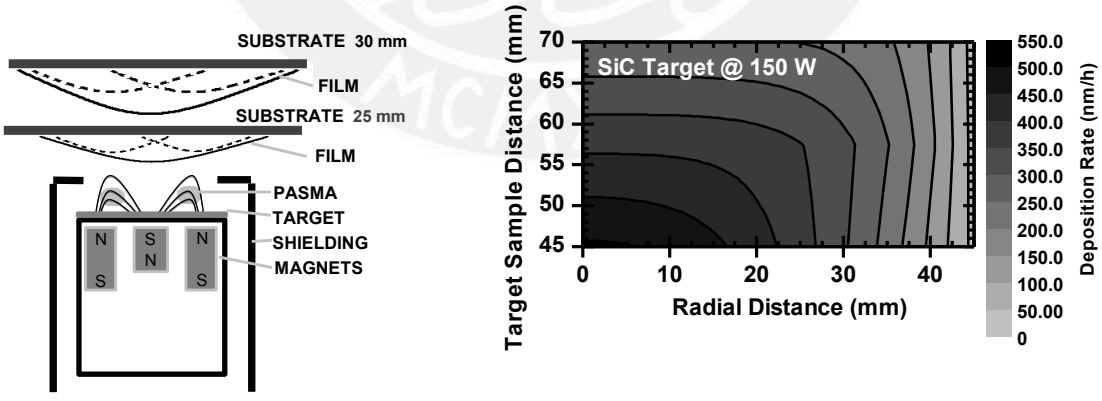

Fig. 3.1.1: Left, Schematic assembly of one magnetron. Two substrate positions with distances at 25 and 30 mm from the target are shown. The expected film thickness distribution is indicated. Right, typical emission pattern of the magnetron with the SiC target at 150 W [24].

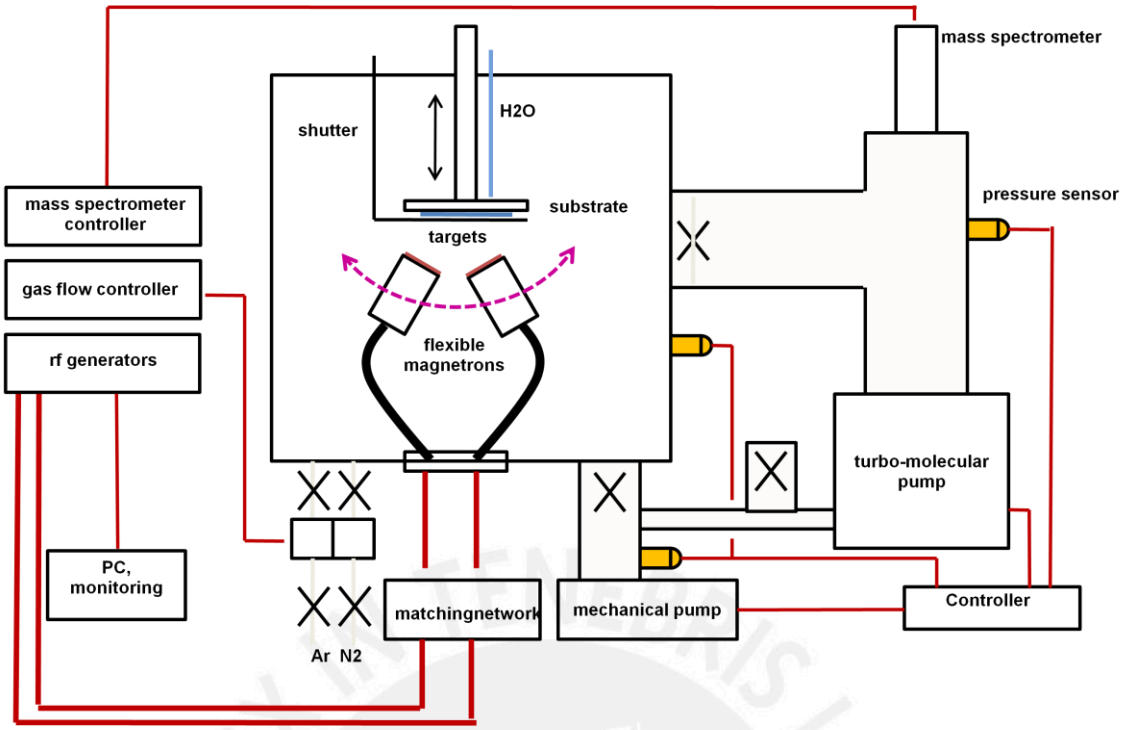

Figure 3.1.2: Schematic of the film production system. The main chamber can reach a pressure of 10×10^{-6} mbar in about one hour. This is the base pressure for the film production. The parameters, power, pressure, gas flow and time are monitored by a computer.

Energy Dispersion Spectroscopy (EDS)

The composition x of the a-$(SiC)_{1-x}(AlN)_x$ films was determined by an EDS system coupled to a scanning electron microscope using the digital X-ray processor DXP-X10P and the multi-channel analyzer NumeriX by Fondis Electronic. Silicon and aluminum peaks in the EDS spectra were well resolved. In the case of CaF_2 substrates, their purity ensures that there is no EDS contribution from the substrate to silicon and aluminum peaks. From the resulting atomic weight percentage of the silicon and aluminum peaks the composition can be determined assuming that the silicon to carbon and the aluminum to nitrogen ratios are 1:1 as it is in the respective targets. Typical EDS spectrum is shown in the figure (3.2.1). The corresponding values are shown in the table (3.2.1).

Table 3.2.1: EDS values corresponding to the spectrum shown in the figure (3.2.1), x = 0.47.

Elt	XRay	Int	Error	K	Kratio	W%	A%
C	Ka	711.1	3.4420	0.1653	0.1140	26.93	40.32
N	Ka	285.1	2.1794	0.1019	0.0703	14.50	18.61
O	Ka	288.0	2.1905	0.0536	0.0370	6.09	6.84
Al	Ka	2122.1	5.9459	0.3150	0.2172	24.07	16.04
Si	Ka	2067.3	5.8686	0.3643	0.2512	28.41	18.19
Total				1.0000	0.6897	100.00	100.00

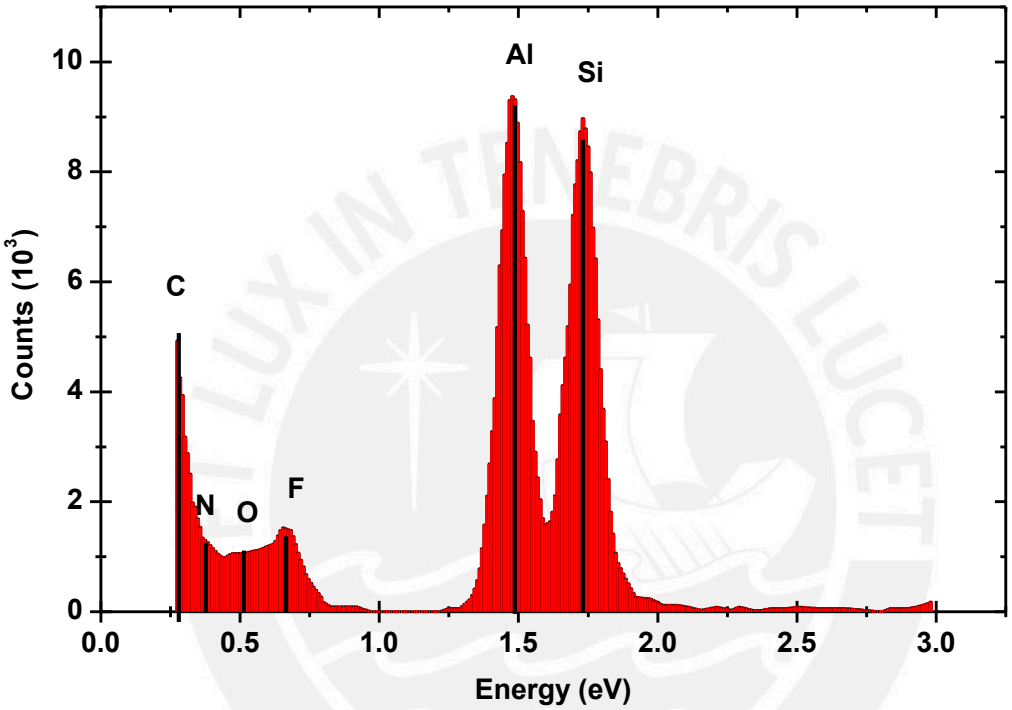

Figure 3.2.1: Typical EDS spectrum of a sample grown on CaF_2. The typical parameters are: magnification x430, voltage of 6kV, measuring time 60 sec. This sample was sputtered with gold to improve the surface conductivity.

Annealing treatment

The annealing treatment of the samples took place in a quartz tube inside an oven tube with three heating stages which can be heated up to 1200°C. The quartz tube was evacuated down to 4×10^{-5} mbar. After the operating temperature was reached, the quartz tube with the samples under treatment was moved rapidly inside the oven (shock tempering). The annealing time for each annealing step was 30 min and the same samples were used for the next annealing steps (isochronal annealing).

Transmission measurements

The transmission spectra of our samples were measured using the double beam photo-spectrometers models Lambda 2 UV/VIS/NIR and Lambda 19 UV/VIS/NIR of Perkin Elmer in the ranges of 190-1100 nm and 200-3000 nm, respectively with a spectral resolution of 1 nm. Absorption coefficients up to 240000 cm^{-1} were recorded.

Typical transmission of our samples is shown in the figure (3.3.1), as we will see in the next chapter this kind of transmission is not suitable to be used with the common methods for the calculation of the optical constants. Details of the methods will be presented in the next chapter.

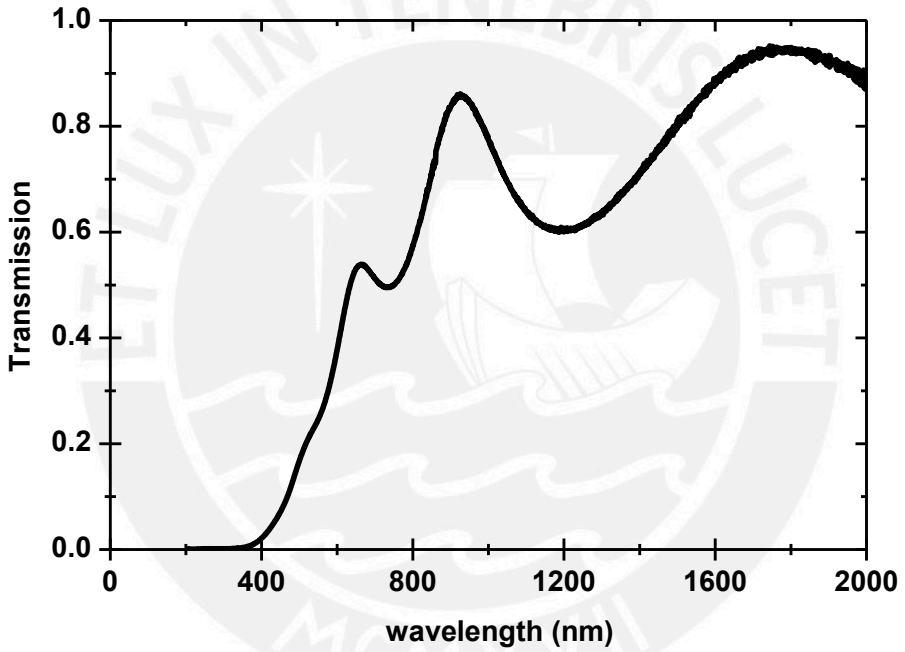

Figure 3.3.1: Typical transmission spectrum of our samples with a thickness of 356.14 ± 0.13 nm and composition of x = 47%. The measure was made using the spectro-photometer Lambda 19 UV/VIS/NIR of the company Perkin Elmer, in the University of Erlangen-Nürnberg in Germany. The thickness was extracted from the transmission spectra with a modified method proposed in the next chapter.

Chapter IV

Bandgap determination

In this chapter we will expend effort in develop our characterization method. The goal is to determine the optical bandgap accurately for different compositions of a-$(SiC)_{1-x}(AlN)_x$ thin films. Therefore the determination of the absorption coefficient especially for the high energy range is necessary. For this a common method will be presented, discussed and modify for our aims. It is important to remark that in the second section of the chapter two (Fundamental absorption) we have already seen some of the problems in the determination of the optical bandgap. In the following sections this issue will be also treated.

Optical constants determination for solids (polished bulk)

In the case of a polished bulk material i.e. Si, SiC, AlN, etc., the determination of the absorption coefficient can be easily perform by using a spectrophotometer. The light passes through the material and a transmission spectrum is recorded, from this spectrum it is always possible to use the Lambert's law $I(\lambda) = I_0(\lambda)e^{-\alpha(\lambda)\,d}$ to obtain the absorption coefficient. The transmission $T(\lambda)$ is obviously associated to the light intensity by $T = I/I_0$ and therefore we can write the absorption coefficient as a function of the transmission spectra by $\alpha = -\ln(T)/d$, the thickness d can be measured by any physical method available.

If we would like to obtain the refractive index n of the material directly from a transmission spectrum measurement T we can use the equation (4.1.1) obtained from the electromagnetism theory [26], it relates the refractive index with the transmission spectrum, and therefore the refractive index can be written as a function of the transmission according to the equation (4.1.2).

$$T = \frac{(1-R)^2}{1-R^2} \qquad (4.1.1)$$

With $R = (n-1)^2/(n+1)^2$

$$n = \frac{1}{T} + \left(\frac{1}{T^2} - 1\right)^{1/2} \qquad (4.1.2)$$

We have shown that it is possible to find the absorption coefficient and the refractive index from a single transmission spectra measurement. However, in the present case we have thin films of 200 to 1000 nm thickness deposited on a 0.5 to 1 mm thick transparent substrate. The procedure to obtain the optical constants is far more complicated than the case presented above.

Optical constants determination for thin films on transparent substrates

In the case of a thin film deposited on a transparent substrate the procedure above is different. It is not possible to obtain the absorption coefficient directly from the transmission spectrum using the Lambert's law, because there is an interference pattern due to the refractive behavior of the light when it passes through the film and the substrate (see figures 4.2.1 and 3.3.1). The equation that relates the transmission with the rest of the optical constants and therefore describes the curve in the figure (4.2.1) is much more complicated than the ones presented in the later section (see equation 4.2.1).

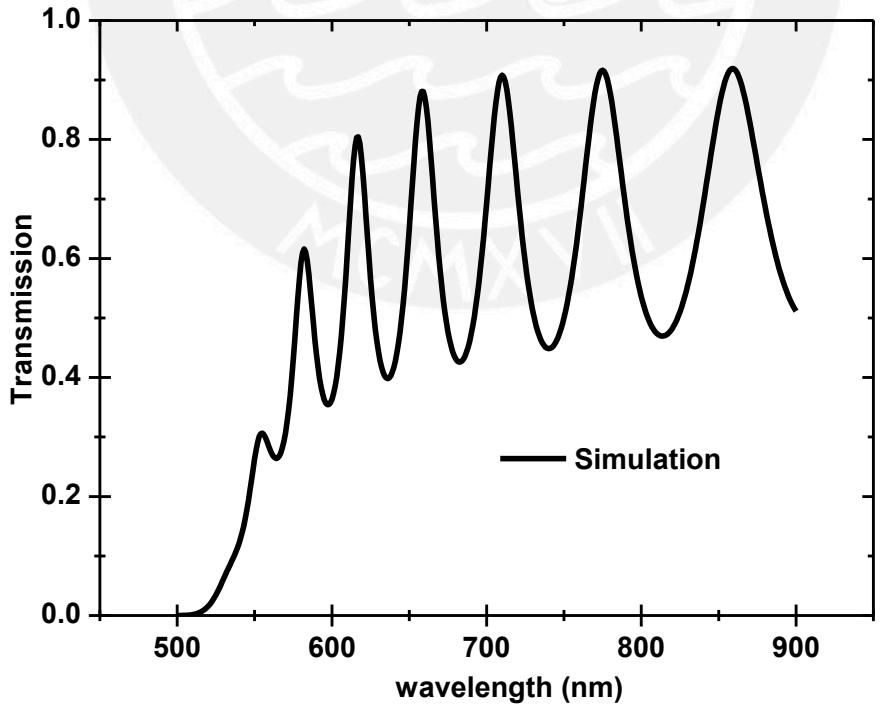

Figure 4.2.1: Typical transmission spectrum of a thin film-substrate system. The curve was simulated using a substrate with a refractive index $s = 1.51$, a film thickness $d = 1000$ nm and refractive index and absorption coefficient $n = 3 \times 10^5/\lambda^2 + 2.6$, $\log \alpha = 1.5 \times 10^6/\lambda^2 - 8\ \mathrm{nm}^{-1}$, typical values of *a*-Si:H, values obtained from reference [27].

$$T = \frac{Ax}{B - Cx + Dx^2} \tag{4.2.1}$$

$$\begin{aligned} A &= 16s(n^2 + \kappa^2) \\ B &= [(n+1)^2 + \kappa^2][(n+1)(n+s^2) + \kappa^2] \\ C &= [(n^2 - 1 + \kappa^2)(n^2 - s^2 + \kappa^2) - 2\kappa^2(s^2 + 1)\,]2\cos\phi \\ &\quad -\kappa[2(n^2 - s^2 + \kappa^2) + (s^2 + 1)\,(n^2 - 1 + \kappa^2)]2\sin\phi \\ D &= [(n-1)^2 + \kappa^2][(n-1)(n-s^2) + \kappa^2] \\ x &= e^{-\alpha d} \end{aligned} \tag{4.2.1.a}$$

$$\begin{aligned} \kappa &= \frac{\lambda\alpha}{4\pi} \\ \phi &= 4\pi nd/\lambda \end{aligned} \tag{4.2.1.b}$$

Where κ is the extinction coefficient, s the refractive index of the substrate and ϕ is related to the basic interference equation $2nd = m\lambda$ by $\phi = 2\pi m$, for the integers values of m, ϕ is an integer multiple of 2π. This relation is used later to calculate the thickness of the films, and will be explained in more detail.

Swanepoel method

To overcome the problem of calculating the optical constants from a single transmission measurement a straight forward method was proposed by R. Swanepoel (1983) [27] developing the previous work of Manifacier *et al* (1976) [28]. In this section the Swanepoel method (also known as envelope method) to determine the optical constants and the thickness of thin films by using a single transmission measurement will be developed, explained and discussed in detail.

Swanepoel's idea was first to reduce the equation (4.2.1) in a less complicated equation by the approximation of $\kappa/n \ll 1$ (see equation 4.2.1.1). This approximation can be used in most of the range of study. Secondly, the resulting maximums and minimums due to the interference effect of the transmission spectrum can be described by the equation (4.2.1.1) for the special cases of $\cos\phi = \pm 1$ and therefore two new equations (4.2.1.2) that only describe the maximums and minimums are found. Swanepoel had the idea to consider these equations as continuous functions of the wavelength. These functions T_M and T_m are the envelopes of the transmission spectrum and in principle it is possible to construct them by using the extremes of interference (see figure 4.2.1.1). The interference pattern far from being an annoying effect that doesn't allow us to measure the absorption of the material properly, it becomes an important tool that provide us with the necessary information to obtain the optical constants.

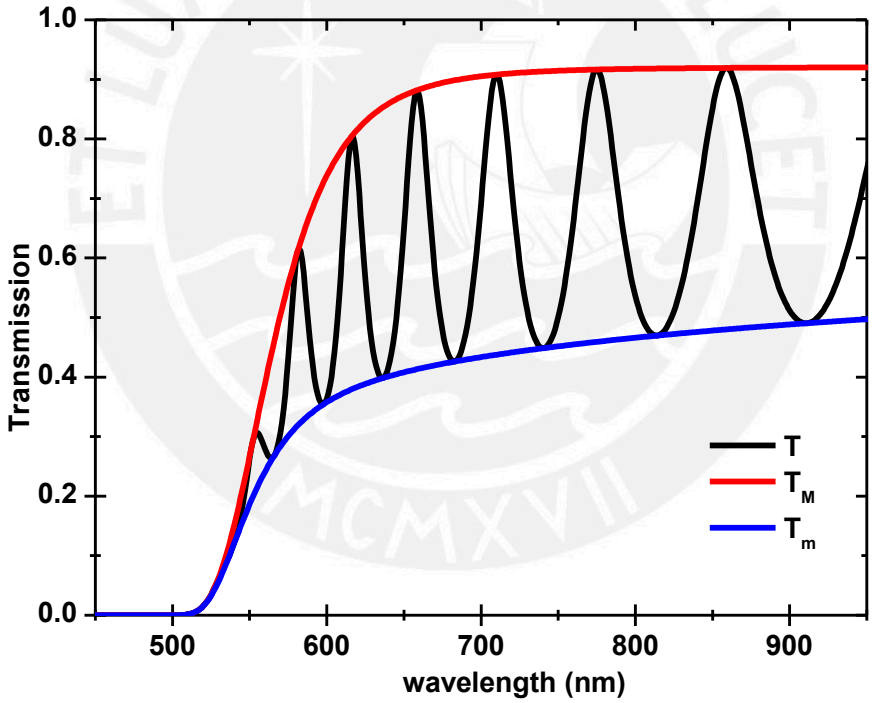

Figure 4.2.1.1: T_m and T_M curves plotted along with the transmission spectrum. It is possible to construct the envelopes properly as long as there are well defined interference fringes.

$$T = \frac{Ax}{B - Cx\cos\phi + Dx^2} \qquad (4.2.1.1)$$

$$A = 16sn^2$$
$$B = (n+1)^2(n+1)(n+s^2)$$
$$C = 2(n^2-1)(n^2-s^2) \qquad (4.2.1.1.a)$$
$$D = (n-1)^2(n-1)(n-s^2)$$
$$x = e^{-\alpha d}$$

$$T_M = \frac{Ax}{B - Cx + Dx^2} \qquad (4.2.1.2.a)$$

$$T_m = \frac{Ax}{B + Cx + Dx^2} \qquad (4.2.1.2.b)$$

Swanepoel decided to divide the spectrum in three regions, a transparent region, a weak and medium absorbing region and one of strong absorption. He did this in order to establish a set of equations obtained from the equations (4.2.1.1) and (4.2.1.2) in each region for the calculation of the optical constants. We will see later that one set of equations is enough to treat the whole spectrum.

The transparent region is characterized by the fact that the absorption coefficient in this region can be approximated to zero $\alpha \approx 0$, therefore the equations (4.2.1.2) can be reduced to the following equations (4.2.1.3). From the equation (4.2.1.3.a) the refractive index of the substrate s is obtained in the same way as the refractive index of polished bulk in the equation (4.1.2), and from the equation (4.2.1.4.b) the refractive index of the film is found according to its equivalent form shown in the equation (4.2.1.3.c) with $M = 2s/T_m - (s^2+1)/2$.

$$T_M = \frac{2s}{s^2+1} \qquad (4.2.1.3.a)$$

$$T_m = \frac{4n^2 s}{n^4 + n^2(s^2+1) + s^2} \qquad (4.2.1.3.b)$$

$$n = \left[M + (M^2 - s^2)^{1/2}\right]^{1/2} \qquad (4.2.1.3.c)$$

In the weak and medium absorption region the absorption coefficient has to be taken into account $\alpha \neq 0$, $x < 1$. Following the Swanepoel method [27], the equations (4.2.1.1) and (4.2.1.2) are used to find an expression for the refractive index as a function of the envelopes and then solve the equations for the absorption coefficient.

Let us subtract the reciprocals of the equations (4.2.1.2). The result is shown in the equation (4.2.1.4) below.

$$\frac{1}{T_m} - \frac{1}{T_M} = \frac{2C}{A} \qquad (4.2.1.4)$$

By substituting the equations (4.2.1.1.a) into the equation (4.2.1.4) and solving for the refractive index n we find a relation between the envelopes T_m, T_M, the refractive index of the substrate s and the refractive index of the film n in the equation (4.2.1.5) with $N = 2s(T_M - T_m)/(T_m T_M) + (s^2 + 1)/2$, this result is equivalent to the result of the reference [28].

$$n = \left[N + (N^2 - s^2)^{1/2}\right]^{1/2} \qquad (4.2.1.5)$$

Once $n(\lambda)$ is known, all the constants of equation (4.2.1.1.a) are known and therefore the equation (4.2.1.1) can be used to solve x. There are many ways to solve x, it is not our aim to show each of the possible equivalent solutions for x that Swanepoel developed, but here we will show one of those ways that Swanepoel developed in his paper and that is equivalent to a well known expression usually used in similar studies.

Let us start with the free interference transmission T_α, this curve can be calculated from the interference fringes by integrating the equation (4.2.1.1) between a maximum and an adjacent minimum that is for ϕ between 0 and π.

$$T_\alpha = \frac{1}{\pi}\int_0^\pi \frac{Ax}{B - Cx\cos\phi + Dx^2}\,d\phi \qquad (4.2.1.6)$$

As suggested by Swanepoel, a narrow integration region where all the parameters are taken as constants, the solution of the integral in equation (4.2.1.6) yields to the equation (4.2.1.7).

$$T_\alpha = \frac{Ax}{[(B - Cx + Dx^2)(B + Cx + Dx^2)]^{1/2}} \tag{4.2.1.7}$$

Using the equations (4.2.1.2) into the equation (4.2.1.7) we find that the free interference transmission is just the geometric mean of the envelopes T_M and T_m (see equation 4.2.1.8).

$$T_\alpha = \sqrt{T_m T_M} \tag{4.2.1.8}$$

The equation (4.2.1.8) is a useful result in the sense that we can solve the equation (4.2.1.7) for x as function of the free interference transmission and obtain the free interference transmission directly from the constructed envelopes. By solving x with the equation (4.2.1.7) we obtain, following the notation of Swanepoel, the equation (4.2.1.9).

$$x = \frac{\{G - [G^2 - (n^2 - 1)^6(n^2 - s^4)^2]^{1/2}\}^{1/2}}{(n - 1)^3(n - s^2)} \tag{4.2.1.9}$$

with

$$G = \frac{128n^4s^2}{T_\alpha^2} + n^2(n^2 - 1)^2(s^2 - 1)^2 + (n^2 - 1)^2(n^2 - s^2)^2$$

The equation (4.2.1.9) is equivalent to an expression found earlier by Connel and Lewis (1973) [29] (see equations 4.2.1.10) and used in several works related to this kind of study [30-33].

$$x = \frac{\left[P + [P^2 + 2QT_\alpha(1 - R_2R_3)]^{1/2}\right]}{Q} \tag{4.2.1.10.a}$$

$$P = (R_1 - 1)(R_2 - 1)(R_3 - 1) \tag{4.2.1.10.b}$$

$$Q = 2T_\alpha(R_1R_2 + R_1R_3 - 2R_1R_2R_3)$$

$$R_1 = \left(\frac{1-n}{1+n}\right)^2$$

$$R_2 = \left(\frac{n-s}{n+s}\right)^2$$

$$R_3 = \left(\frac{s-1}{s+1}\right)^2$$

From the equations (4.2.1.10) and having the free interference transmission T_α, x can be calculated, and then to obtain the absorption coefficient from x we can use the expression in equation (4.2.1.1.a), that is $x = e^{-\alpha d}$. Now, for this we need the thickness d. It can be calculated from the basic equation of interference fringes, the equation (4.2.1.11).

$$2nd = m\lambda \tag{4.2.1.11}$$

For two adjacent maximums we have two values of the refractive index for the corresponding wavelength, and then the equation (4.2.1.11) can be written as the equations (4.2.1.12).

$$\begin{aligned} 2n_1d &= m\lambda_1 \\ 2n_2d &= (m+1)\lambda_2 \end{aligned} \tag{4.2.1.12}$$

Where n_1 is the refractive index for the wavelength λ_1 that corresponds to the position of one maxima and n_2, λ_2 to the adjacent one. By solving the equations (4.2.1.12) for the thickness d we find the equation (4.2.1.13).

$$d = \frac{1}{2}\left(\frac{\lambda_1\lambda_2}{\lambda_1n_2 - \lambda_2n_1}\right) \tag{4.2.1.13}$$

It is important to remark that the transmission is a function of the wavelength, the absorption coefficient, the refractive index, and the thickness $T(\lambda, \alpha, n, d)$ and also are the envelopes $T_m(\lambda, \alpha, n, d)$ and $T_M(\lambda, \alpha, n, d)$. In this sense the envelopes complete the

system of equations necessary to solve n, α and d as functions of the wavelength (the thickness is of course a constant).

In the strong absorbing region the interference pattern disappears and therefore is not possible to calculate n and x separately. Swanepoel suggest to extrapolate the refractive index using the values found earlier and therefore calculate the corresponding function x.

Another useful result of Swanepoel is the curve that passes through the inflexion points of the transmission spectrum T_i, it was found by Swanepoel as a function of the envelopes, that is $T_i = 2T_m T_M/(T_m + T_M)$.

In principle, from the envelopes it is possible to use the equations corresponding to the weak absorbing region to calculate the optical constants in the whole range as long as the envelopes do not become equal, which is in the region where an interference pattern is still found.

After presenting the Swanepoel's method, in the following paragraphs we will review some problems with it. It is important to note that the Swanepoel's method cannot be applied to every transmission spectrum, although the equations (4.2.1.1) and (4.2.1.10) are always valid.

There are two main problems with the Swanepoel's method. The first one, the envelopes are constructed using the maximums and minimums of the transmission spectrum and these extremes are shifted due to the absorption effect in the high energy region (see figure 4.2.1.2) and therefore the envelopes constructed will not match the true envelopes. The second problem, the envelopes can only be constructed when a considerable number of fringes are present in the transmission. This is not the case for films with a thickness around 300 nm where the number of extremes is very low and therefore there is much space between extremes and the construction of the envelopes becomes a difficult matter, (see figure 4.2.1.3). These problems where noted by D. Pelman and P. Frederic (2003) [34]. "There is not a 'right' way to construct the envelopes between interference fringes. ...", "The envelopes should ideally be constructed from the tangent points touching the transmission curve, not from the interference extremes: it is easy to see that, especially in a region where the

transmission is changing fast...". This issue will be treated in the next section and an alternative will be proposed to overcome part of these problems.

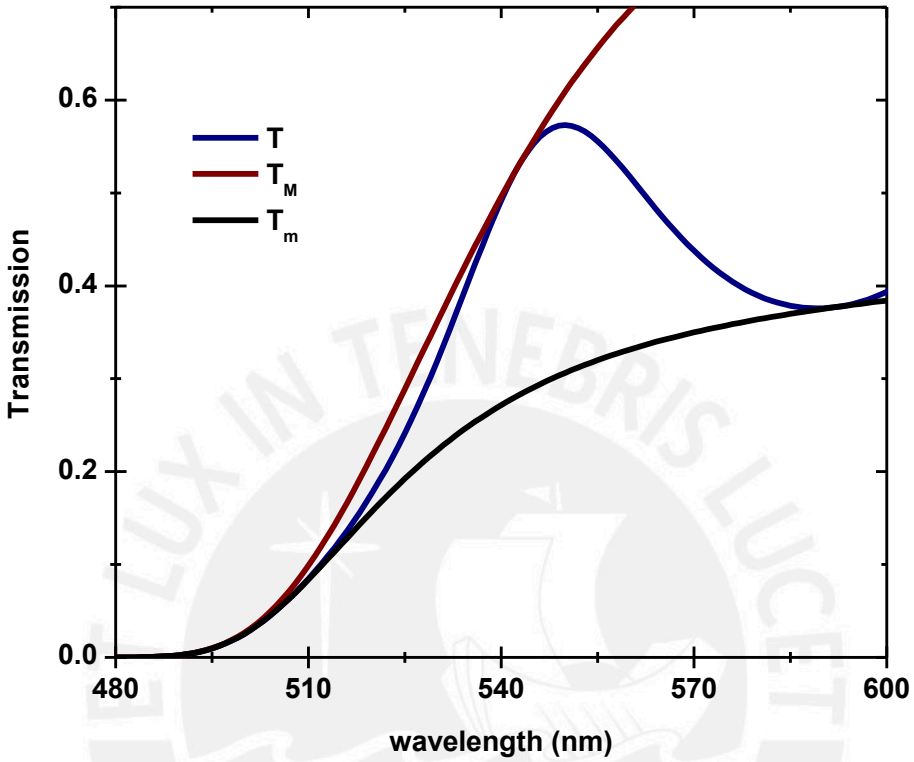

Figure 4.2.1.2: Rescaled T_m and T_M curves plotted along with the transmission spectrum for a film with a thickness of 300 nm. Note how due to the absorption effect the extremes of the transmission does not belong to the envelopes, this shift in the extremes does not allow a proper construction of the envelopes because the envelope pass through a tangent point.

An important remark is that for applying the Swanepoel method a considerable number of interference fringes must appear in the transmission spectrum and this implies at the same time a thicker sample (see figure 4.2.1.3), but for thicker samples it is more difficult to measure the optical bandgap in the sense that less data of the absorption coefficient in the high energy region will be available. As we will see later this compromise limits the use of the Swanepoel's method in our samples.

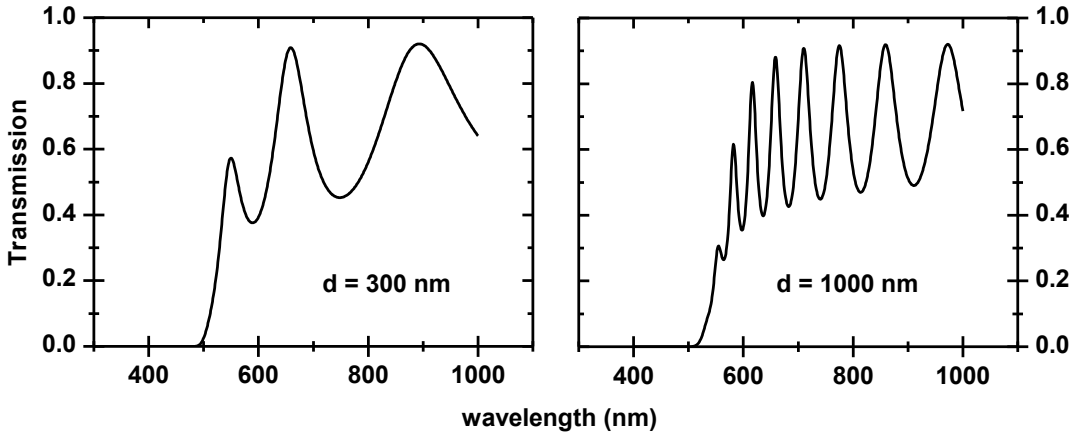

Figure 4.2.1.3: Simulation using two different thicknesses. The thinner film with low number of interference fringes will not allow the proper construction of the envelopes, contrary to the thicker film.

Manipulation method

As it was mentioned in the last section, there are two main problems with the Swanepoel method. The aim of this section is to propose a solution to overcome part of these problems, especially to find the optical bandgap. First we will give an approach of how to find a better value of the extremes for building the envelopes in the high absorption region. Then we will use a set of equations and propose a recursive routine to find the right values of thickness, absorption coefficient and refractive index.

As we know, in the region of strong absorption it is not possible to use the extremes of the transmission to build the envelopes since the extremes do not lay in the envelopes (see figure 4.2.1.2), but we can get closer to the right values with the following idea: the tangent points or right extremes values that belong for example to the envelope T_M are the extremes of the curve defined by T/T_M. Of course we do not know T_M yet, but in the strong absorption region a curve closer to this one is the curve defined by the inflexion points T_i. To illustrate this idea see the figure (4.2.2.1).

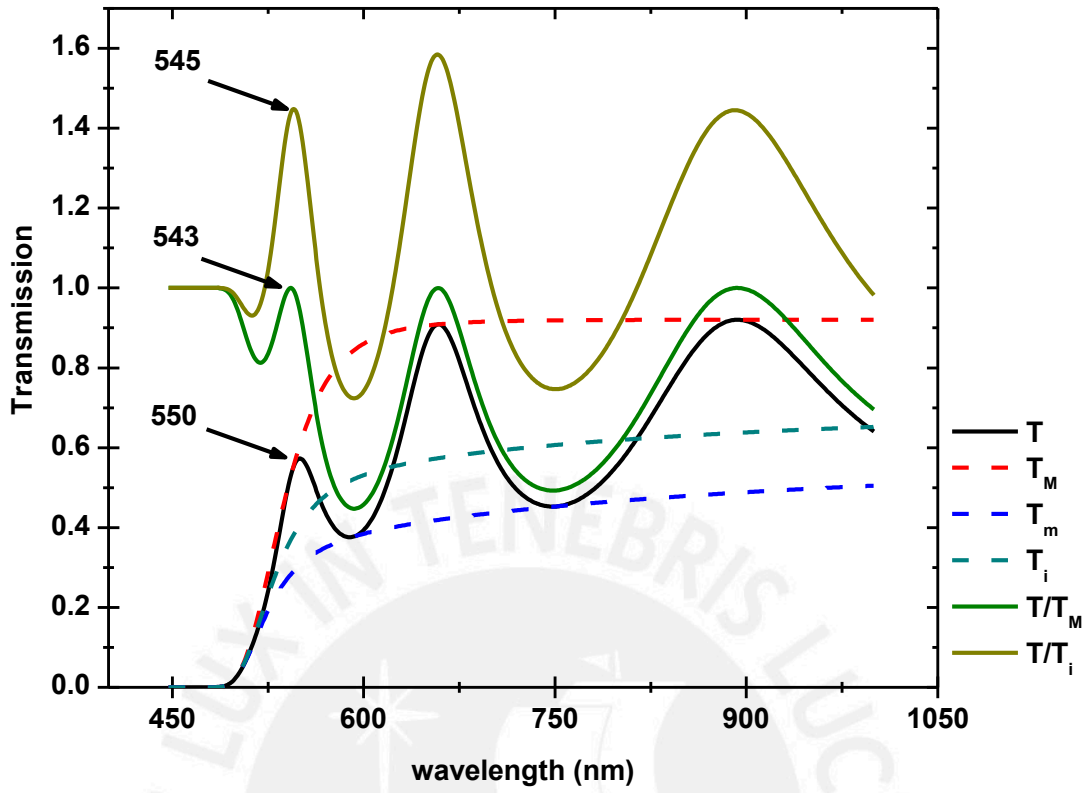

Figure 4.2.2.1: In this graph we show the position of the extreme at 550 nm that belongs to the transmission but no to the envelope. From the curve defined by T/T_M the position of the extreme at 543 nm that belongs to the envelope is shown, and the extreme from the curve defined by T/T_i at 545 nm is also shown.

In the case shown in the figure (4.2.2.1) for three apparent maximums we have six inflexion points to build the T_i curve and to use it for finding close values of the positions of the extremes.

Even with the right positions of the extremes, the construction of the envelopes in the case of films with a low number of interference fringes (that is in our simulation for films with a thickness about 300 nm) is a difficult task, because the large separation between extremes, and therefore the constructed envelopes will not be always suitable to calculate the refractive index. However, with the pseudo-envelopes constructed in those cases the calculated T_α curve is suitable to determine the absorption coefficient. This is the starting point of the manipulation method presented in the following paragraphs. We will use the envelopes constructed to calculate the T_α curve. The refractive index and the thickness will be parameters to find through a fit.

The refractive index can be expressed as a function of the wavelength through the Cauchy dispersion formula (see equation 4.2.2.1). The equation (4.2.2.1) is valid for most of the range of study. Therefore for the refractive index two constant parameters should be found. These parameters p and q will be manipulated along with the thickness d using the equations (4.2.1.10) and (4.2.1).

$$n = p + \frac{q}{\lambda^2} \qquad (4.2.2.1)$$

Now, the problem is reduced to find three parameters fitting the equation (4.2.1) to the measure transmission using the equations (4.2.2.1) and (4.2.1.10). Due to the complexity of the equations it is necessary to give appropriate starting values of these parameters to perform a fit. The parameters are manipulated manually (actually through a well implemented GUI -Graphic User Interface- or graphic tool). The transmission is simulated using the equation (4.2.1) and compared to the measured transmission, the parameters p, q and d are changed till both the simulated and measured transmission fit best. The parameters values found by the manipulation are used as starting values to run a fit of the transmission.

In the material science group of the PUCP we have implemented a program to apply the manipulation method already. The variables p, q and d are manipulated in Mathematica 7.0 till both curves match best and then a fitting algorithm is perform. The extremes can be found by the method explained before or also given manually.

We have tested the method in several samples with different compositions and thicknesses see figure (4.3.2), i.e. the resulting fit for the measured transmission showed in the figure (3.3.1) for a composition of 47% is shown in the figure (4.2.2.2) the fitted curve is plotted in red dashed line to compare them.

.

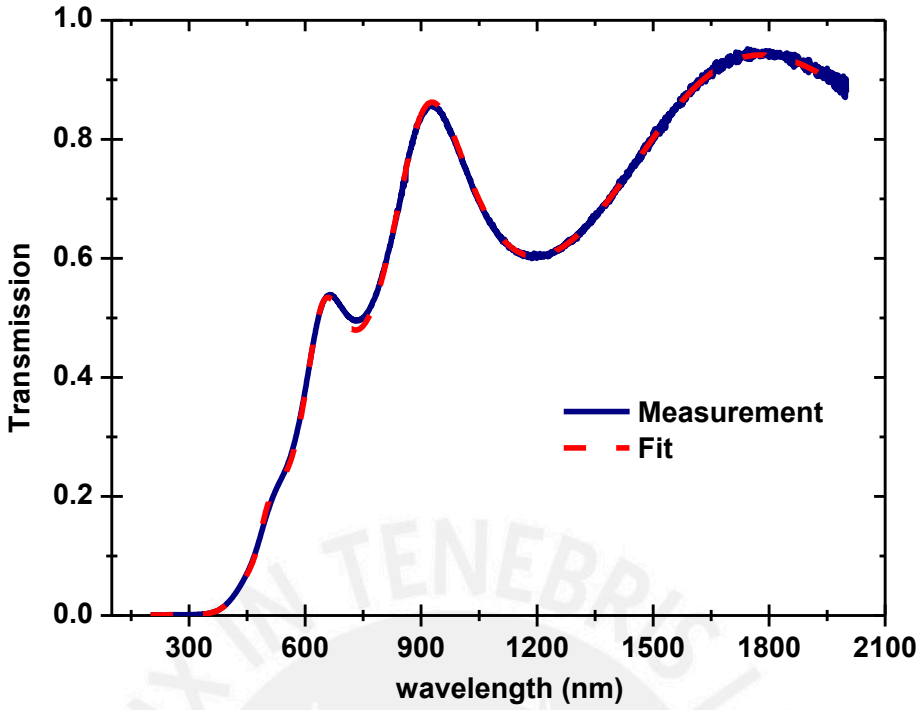

Figure 4.2.2.2: Measured transmission spectrum (blue solid line) and the fitted transmission (red dashed line) using the manipulation method. The parameters found are d = 356.14 ± 0.13 nm, p = 2.48 ± .0009, q= 83329.111 ± .00001 nm^{-1}. The corresponding absorption coefficient is shown in figure (4.2.2.3)

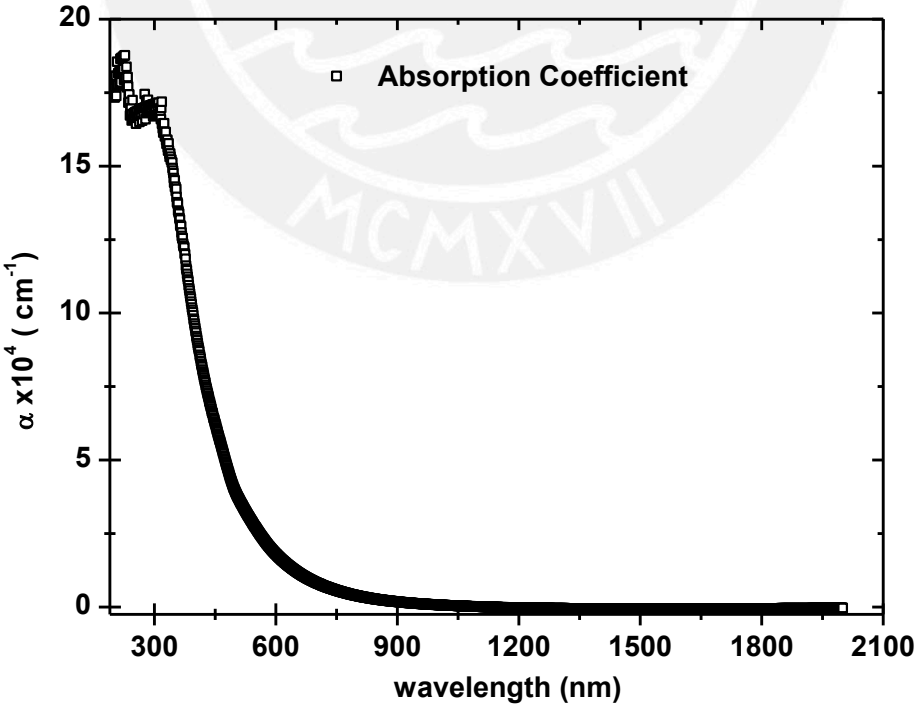

Figure 4.2.2.3: Absorption coefficient corresponding to the data shown in figure 4.2.2.2. It is possible to observe a clear tail between 450 and 900 nm. The region below 350 nm should be ignored for further calculations.

The manipulation method was tested on the Swanepoel's simulation, see figures (4.2.1), (4.2.2.4) and reference [27]. To test the accuracy of the method a comparison of the simulation values with the measured values is shown in table (4.2.2.1). Also the comparison of the measured absorption coefficient with the theoretical absorption coefficient is shown in the figure (4.2.2.5).

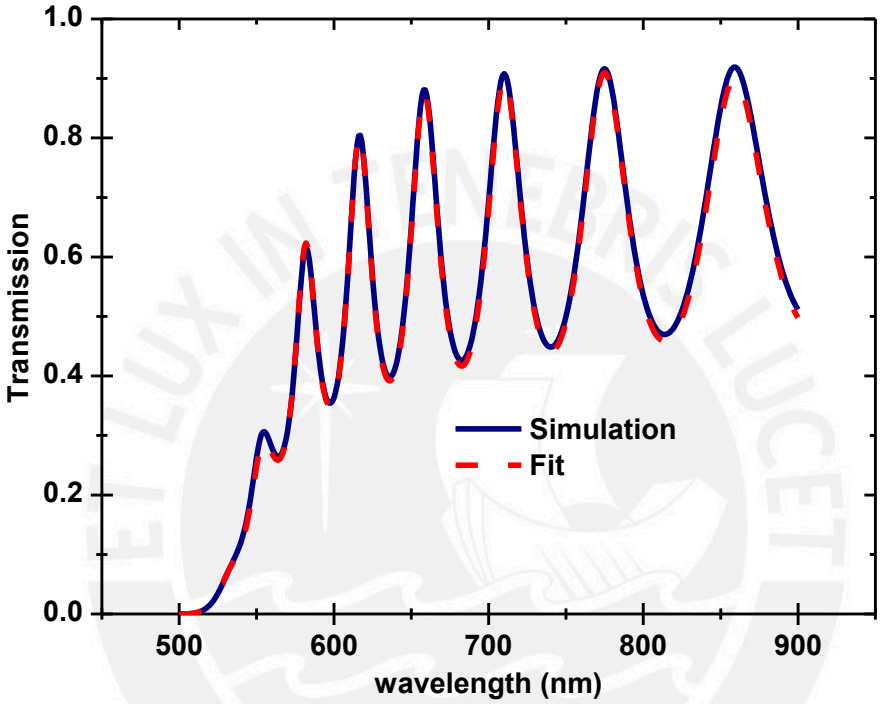

Figure 4.2.2.4: Simulated transmission using a substrate with a refractive index $s = 1.51$, a film thickness $d = 1000$ nm, refractive index $n = 3 \times 10^5/\lambda^2 + 2.6$ and absorption coefficient $\log \alpha = 1.5 \times 10^6/\lambda^2 - 8\ \mathrm{nm}^{-1}$, typical values of a-Si:H, values obtained from reference [27]. And the fitted curve using the manipulation method, the corresponding parameters values are shown in table (4.2.2.1)

Table 4.2.2.1: Comparison between the simulation parameters values from reference [27] and the measured values obtained with the proposed manipulation method.

	Simulation Values	Fit results	Confidence Interval at 95%
d	1000 nm	989.16 ± 1.3691 nm	[986.47, 991.86]
p	2.6	2.63 ± 0.0037	[2.623, 2.637]
q	$3x10^5$ nm^{-1}	$3.02x10^5$ ± 582.9 nm^{-1}	[$3.01\ x10^5$,$3.03\ x10^5$]

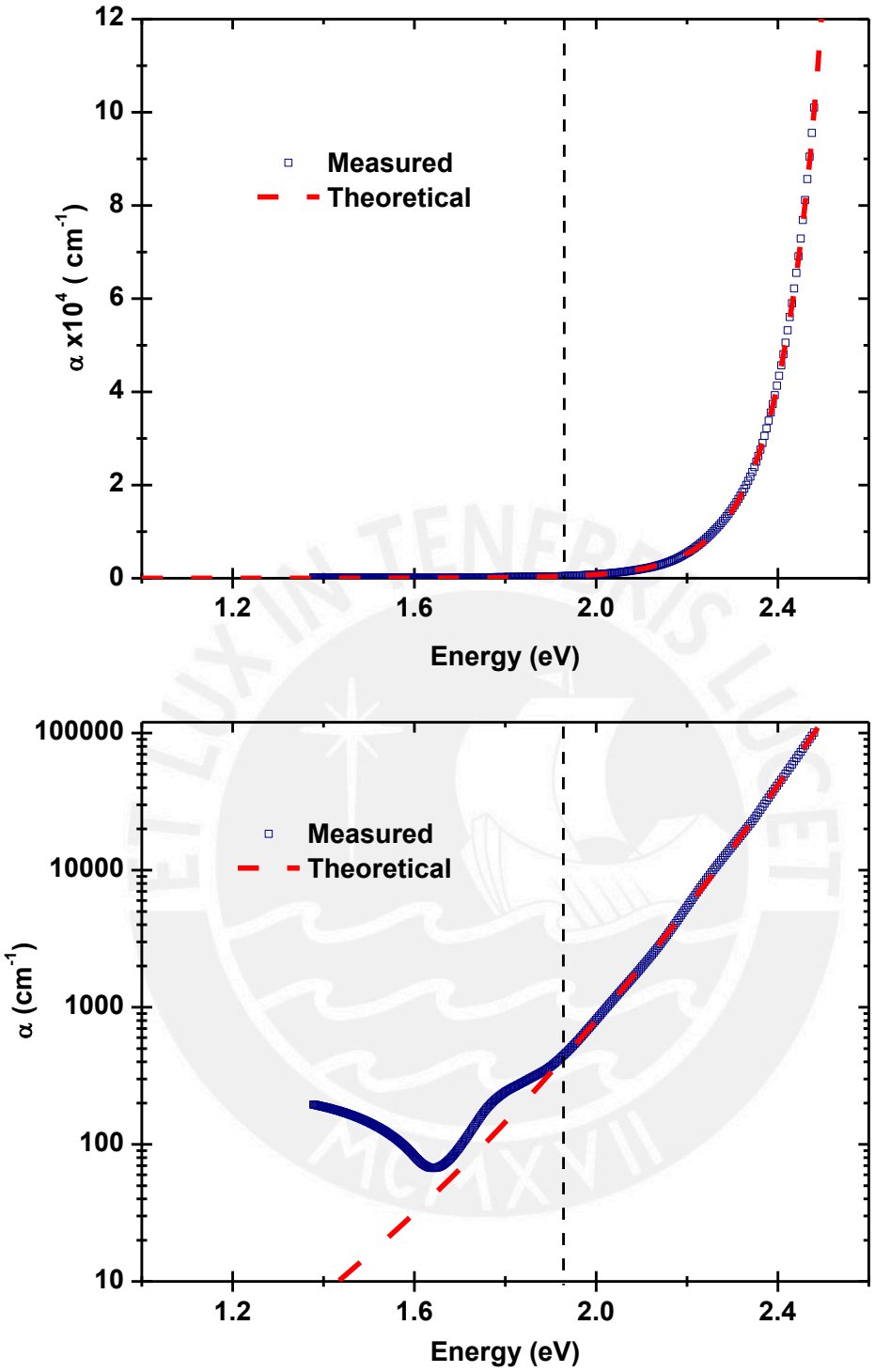

Figure 4.2.2.5: Corresponding absorption coefficient to the simulation, dashed in red, and measured, blue squares. Two different scales are shown. Linear scale: the results seem to fit very well with the theoretical curve. Logarithmic scale: it is possible to identify a disagreement between the measured and the theoretical curves in the low energy region or low absorption region. This is a systematical error that should be taken in to account in the case that a fit on the absorption coefficient might be performed.

Now that we have a method to obtain the optical constants, it is left to obtain the optical bandgap from the absorption coefficient i.e. from the resulting absorption coefficient shown in fig (4.2.2.3). For this two common representations of the absorption coefficient and a model will be used, therefore three bandgaps corresponding to the same sample absorption coefficient are found. This topic will be treated in the next section.

Bandgap determination

Once the best fit between the measured and the simulated transmission is achieved, the absorption coefficient is obtained directly from $x = e^{-\alpha d}$. The optical bandgap can be determined from the absorption coefficient. It is important to remark that for thicker samples less data of the absorption coefficient is available. This feature is illustrated in the figure (4.3.1). For our aims the optical bandgap can only be determined if enough data of the absorption coefficient is available.

The compromise is that thicker films have more interference fringes that can be used to construct the envelopes properly and to calculate the thickness accurately, but at the same time less information of the absorption coefficient is obtained and therefore the calculation of the optical bandgap becomes difficult or even impossible. Thinner films have less interference fringes, and therefore the calculation of the thickness and the construction of the envelopes become a difficult task, but the transmission have information closer to the absorption edge and therefore to the fundamental absorption. Then the calculation of the optical bandgap is possible.

In any case, since we are using the manipulation method which only needs the envelopes for the calculation of the T_α curve. The thickness and refractive index are taken as variables or parameters to find through a fit. Thus we have chance to apply the method to transmission spectrums with a low interference pattern and obtain reliable results. In fact this method was used to determine the thickness of pure AlN and pure SiC films with a low number interference fringes in the transmission spectrum with the aim of determine the emission or deposition rate pattern of the sputtering target [24][25]. The advantage of the method in these cases is that is not destructive and the films are preserved.

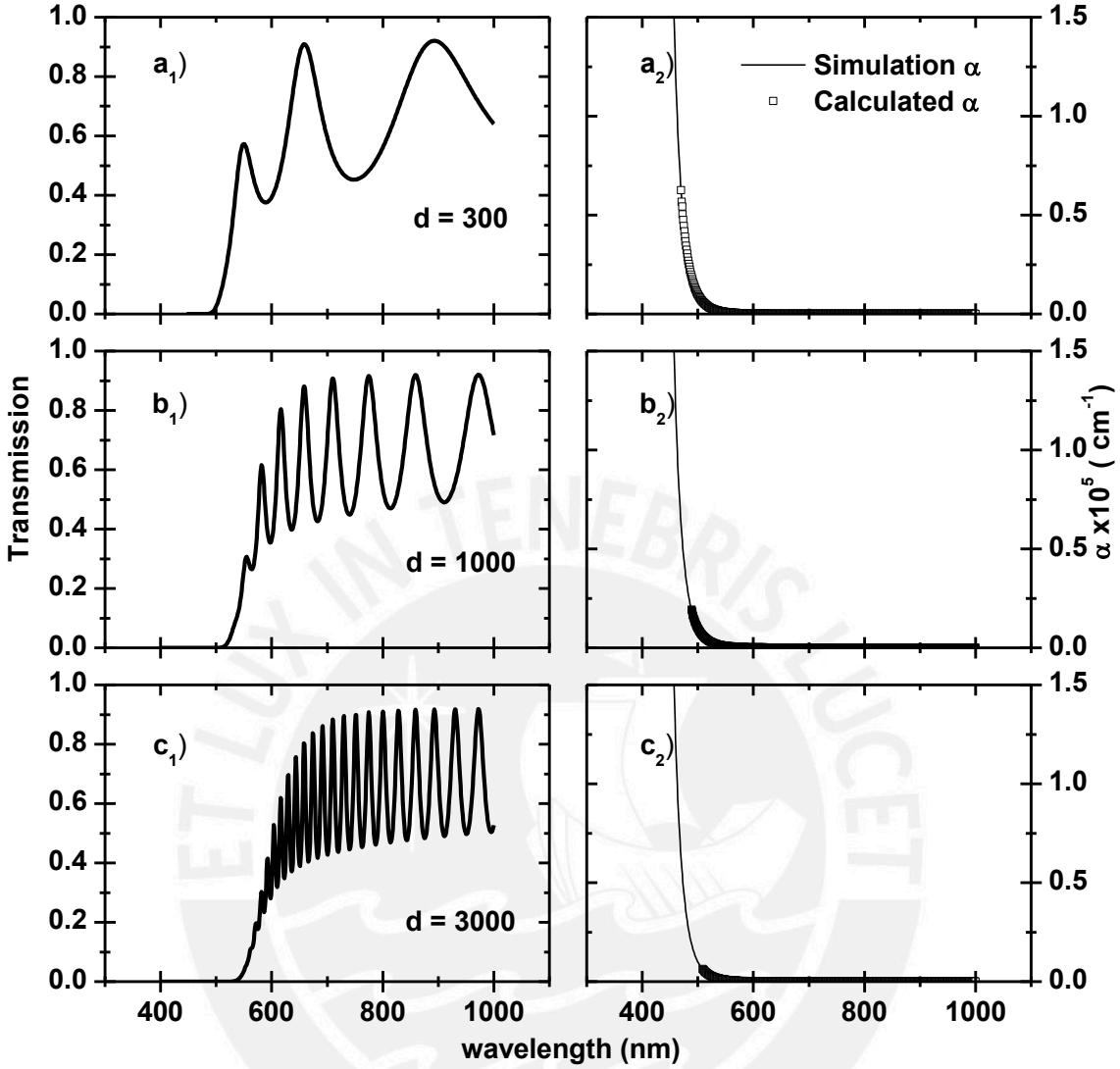

Figure 4.3.1: Set of simulated transmission for three different thicknesses a_1, b_1, c_1, and their respective absorption coefficients a_2, b_2, c_2. The range of the calculated absorption coefficient plotted in squares is reduced along with the increment of the thickness.

We have seen that there are several problems for obtaining the absorption coefficient of a thin film deposited in a transparent substrate. But once we have the absorption coefficient we have to deal with the representation problem for obtaining the optical bandgap. We will use two common representations of the absorption coefficient to determine the optical bandgap, the Tauc plot and the $(\alpha E)^2$ plot [2][4][7][17]. Also we will propose the use of known but no often used model to make a fit and obtain the optical bandgap from it.

In the second section of the Chapter II, fundamental absorption in amorphous solids, an approach to the calculation of the absorption coefficient of an amorphous solid developed by J. Tauc (1968) [7] was presented. It was also mentioned in that section that the Tauc representation might not be the better one to determine the optical bandgap in all the cases and therefore other representations are typically used in the literature [2][17][21][22].

The region where the refractive index decrease towards shorter wavelengths is known as a region of anomalous dispersion and therefore a Kramers Kronig consistent oscillator model to describe it should be used. The imaginary and real parts of the complex refractive index $\tilde{n} = n + ik$ are related each other by the Kramers Kronig relations (KKRs) shown in the equations (4.3.1) where P is the Cauchy principal value [9][22][38].

$$n(\omega) = 1 + \frac{P}{\pi}\int_{-\infty}^{\infty} \frac{\omega' k(\omega')}{\omega' - \omega} d\omega' \qquad (4.3.1.a)$$

$$k(\omega) = -\frac{P}{\pi}\int_{-\infty}^{\infty} \frac{n(\omega') - 1}{\omega' - \omega} d\omega' \qquad (4.3.1.b)$$

The region where the refractive index increases towards shorter wavelengths is known as a region of normal dispersion. The Cauchy dispersion relation accomplishes a normal dispersion and hence the Cauchy-Urbach model can be used to describe the absorption coefficient.

In the Cauchy-Urbach dispersion model the refractive index is described by $n = A + B/\lambda^2 + C/\lambda^4$, and the extinction coefficient is modeled by the equation (4.3.2) often used in ellipsometic analysis [22].

$$k(\lambda) = k_0 \exp\left[\beta\, hc\left(\frac{1}{\lambda} - \frac{1}{\gamma}\right)\right] \qquad (4.3.2)$$

The absorption coefficient can be calculated from the extinction coefficient k by $\alpha = 4\pi k/\lambda$. The absorption coefficient in the energy frame is shown in the equation (4.3.3) where the remaining constants coefficients were absorbed by the scale factor α_0.

The parameter $1/\beta$ is known as the disorder energy [6][11][12][16][18][19][23], and it takes into account the topological and thermal disorder. The parameter E_0 was claimed by D. J. Dunstan [18][19] to be a new material constant, however this parameter is just the true energy gap between the conduction and valence band edges, thus is characteristic of the material itself and it matches the optical bandgap of the material in the crystalline state.

$$\alpha(E) = \alpha_0 E \exp[\beta\,(E - E_0)] \tag{4.3.3}$$

Nevertheless, the calculation of the optical bandgap following this model can be performed as suggested by D. J. Dunstan (who proposed a similar model based on the Tauc representation) [18][19] by the fact that the disorder energy reduces the gap between the conduction and valence band edges creating tail states below the mobility edges.

$$E_g = E_0 - 1/\beta \tag{4.3.4}$$

It is important to note a problem when a fit using the equation (4.3.3) is performed. The parameters α_0 and E_0 are linked and therefore the errors of this two parameters became large. This is easily seen when taking the natural logarithm of the equation (4.3.3) and reordering the terms (see equation 4.3.5). The equation behaves like a straight line, except for the $\ln(E)$ term, with a slope β and intercept $[\ln(\alpha_0) - \beta E_0]$ which in a fit is a finite value and therefore α_0 and E_0 are linked.

$$\ln(\alpha) = [\ln(\alpha_0) - \beta E_0] + \beta E + \ln(E) \tag{4.3.5}$$

When fitting a set of data is necessary to fix one of the parameters α_0 or E_0, i.e. for the absorption coefficient shown in the figure (4.2.2.3), the evaluation with the Tauc-plot the $(\alpha E)^2$-plot and the Cauchy-Urbach model are shown in the figure (4.3.2). We will see in the next chapter that the parameters α_0 and E_0 have a more fundamental meaning.

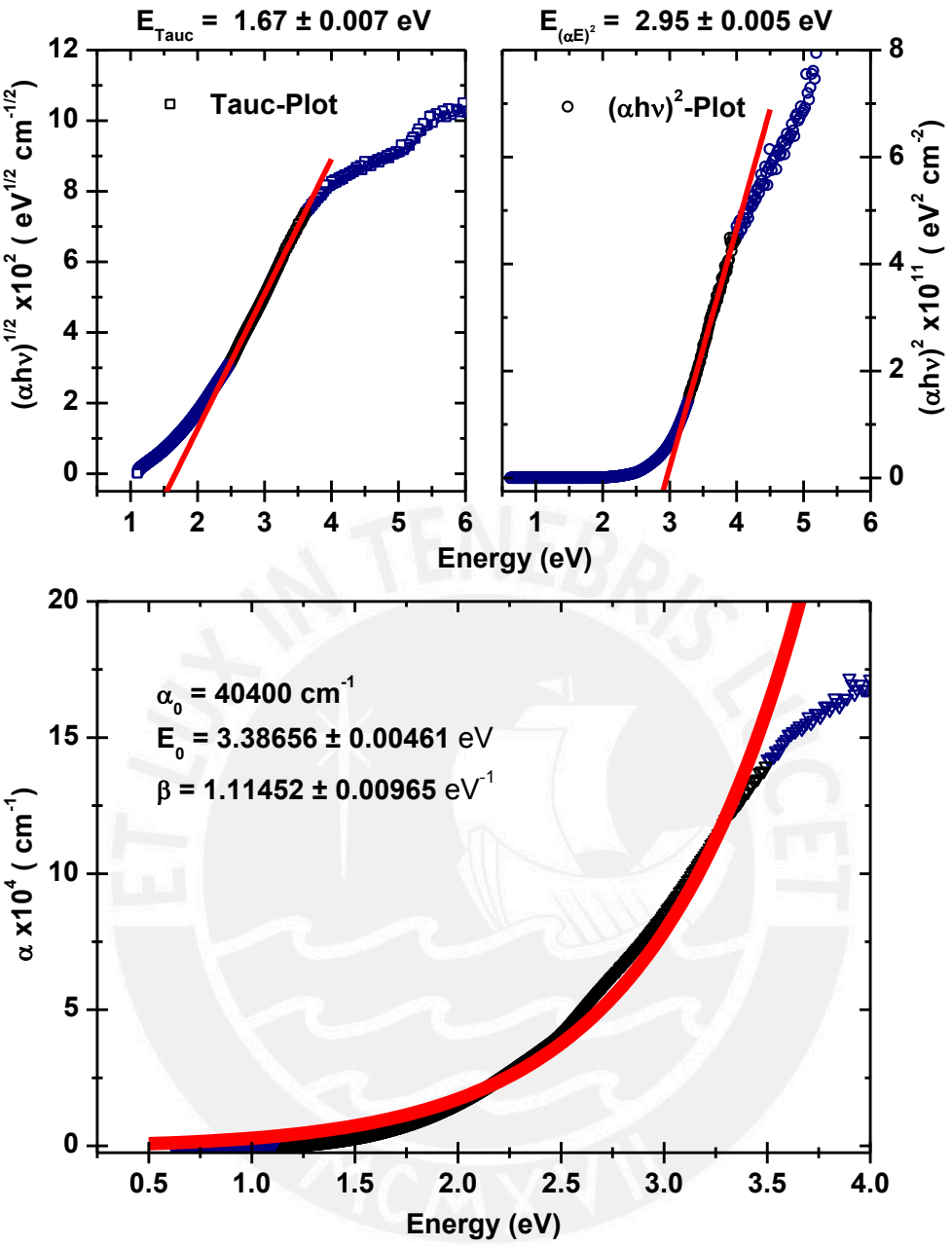

Figure 4.3.2: Bandgap determination using the two typical representations Tauc and $(\alpha E)^2$. And the fit using the Cauchy Urbach model. The parameter α_0 is arbitrarily fixed at 40400 cm^{-1}. β is not linked to any parameter.

To avoid the problem of fixing one of the parameters arbitrarily α_0 or E_0 in the fit of the Cauchy-Urbach model, it is possible to make a global fit as long as enough sets of data of the absorption coefficient of the same material and/or sample are available. Then a global fit (multiple data set) sharing the parameters E_0 and α_0 can be performed without fixing any parameter.

This technique was used in a study of pure *a*-AlN films grown with a Nitrogen atmosphere. Various sets of data of the absorption coefficient where obtained using the manipulation method proposed in this thesis. The samples where annealed at different temperatures and therefore the absorption coefficient with different disorder energies were obtained. The resulting bandgaps will be presented in the last chapter.

Results concerning three samples with different composition and thickness are shown in the figure (4.3.3). The obtained optical bandgap for both representations are in apparent disagreement, there is not a strict way to prove which of them is the right representation, in fact none of them could be the right one. We may find an answer once we plot the bandgaps for each representation against the composition. This topic will be treated in the next chapter.

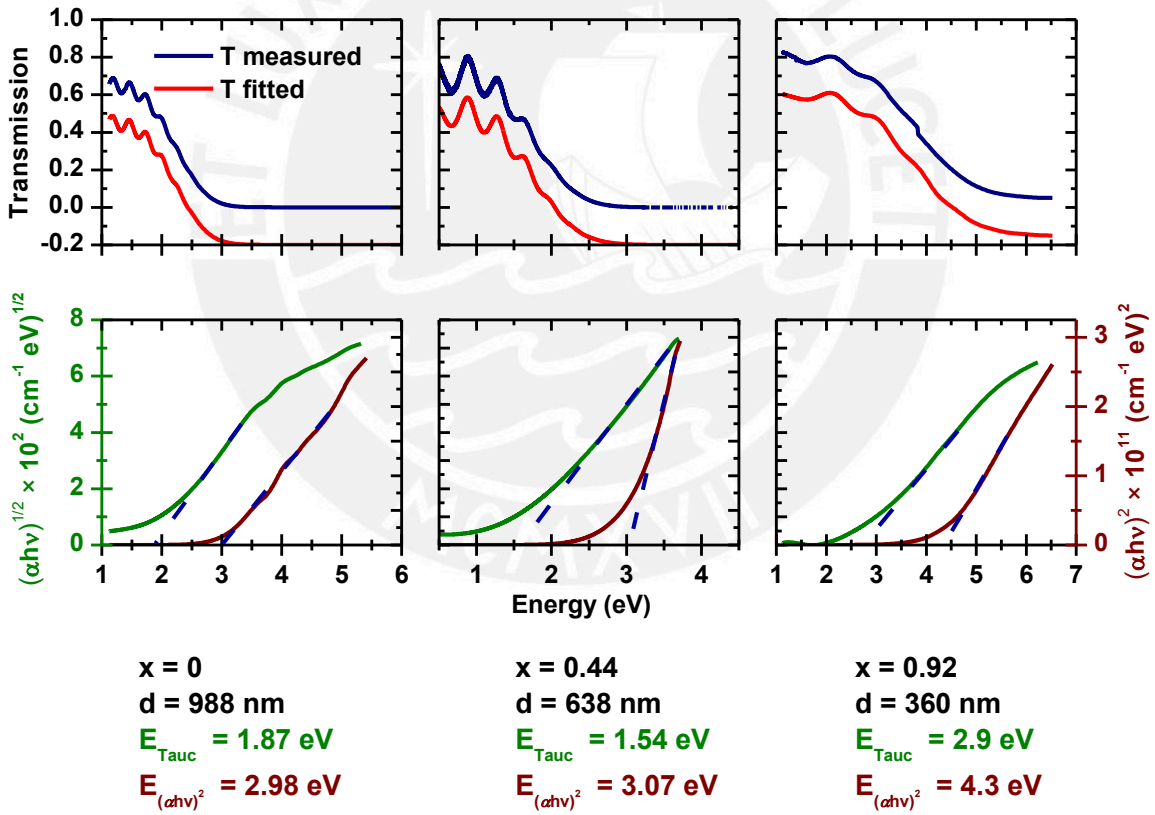

Figure 4.3.3: Fitted transmission of three different samples using the proposed manipulation method, and their respective representations of the absorption coefficient. The transmission fit is plotted at -0.2 to be able to compare it with the measured transmission.

Chapter V

Results and discussion

A method to obtain the optical constants of thin films deposited on transparent substrates was implemented based on the Swanepoel's method. The improvements consist applying the method for the case of films with a low interference fringes in the transmission spectrum and therefore obtain information of the absorption coefficient in the high energy region of films with a thickness around 300 nm for the calculation of the optical bandgap from the fundamental absorption.

This chapter is divided in two main sections. In the first section results concerning the bandgap values for the whole range of compositions of *a*-$(SiC)_{1-x}(AlN)_x$ are shown and the dependence of the optical bandgap with the composition is discussed. In the second section results concerning the optical bandgap and Urbach tail variation through annealing treatments of pure *a*-AlN films are shown and discussed.

Bandgap engineering

As it was mentioned in the last chapter, the determination of the optical bandgap can be done by choosing an appropriate representation of the absorption coefficient with the photon energy and extrapolating the linear part that appears in the respective representation. The fundamental absorption in amorphous films is highly influenced by the presence of localized states which appear in the form of band tails discussed in the chapter two. They are mainly caused by the intrinsic disorder of the material but can also be induced by defects [17]. The determination of the optical bandgap could be very difficult or even impossible if the linear part of the fundamental absorption used to determine the optical bandgap is significantly reduced by these band tails. For example in the figure (2.2.3.3) it seems that there is only information of the absorption coefficient in the tail region and probably away from the fundamental absorption and therefore after an annealing treatment and a reduction of the tails the optical bandgap is no longer able to be calculated since no extrapolation is possible for the $(\alpha E)^2$ representation.

The most common representation of the absorption coefficient for the determination of the bandgap for amorphous materials is known as the Tauc-plot [7], where the dependence of the absorption coefficient with energy is parabolic: $\alpha = C\,(E - E_{Tauc})^2/E$. In this formula, E_{Tauc} is the Tauc-gap and represents a measure of the optical bandgap. Another commonly used representation is induced by the $\alpha = C\,(E - E_g)^{1/2}/E$ dependency, here called the $(\alpha hv)^2$ plot [2][22]. Generally both methods lead to different bandgap values, indicating that they are only reference values of the true mobility edge of the amorphous state. In order to compare our values with those in the literature we apply systematically both methods of bandgap extraction as it was shown in the figure (4.3.3), the resulting values of the bandgap versus composition for samples covering most of the composition range are shown in the figure (5.1.1) along with the bandgap values of *a*-AlN and *c*-$(SiC)_{1-x}(AlN)_x$ obtained from the literature.

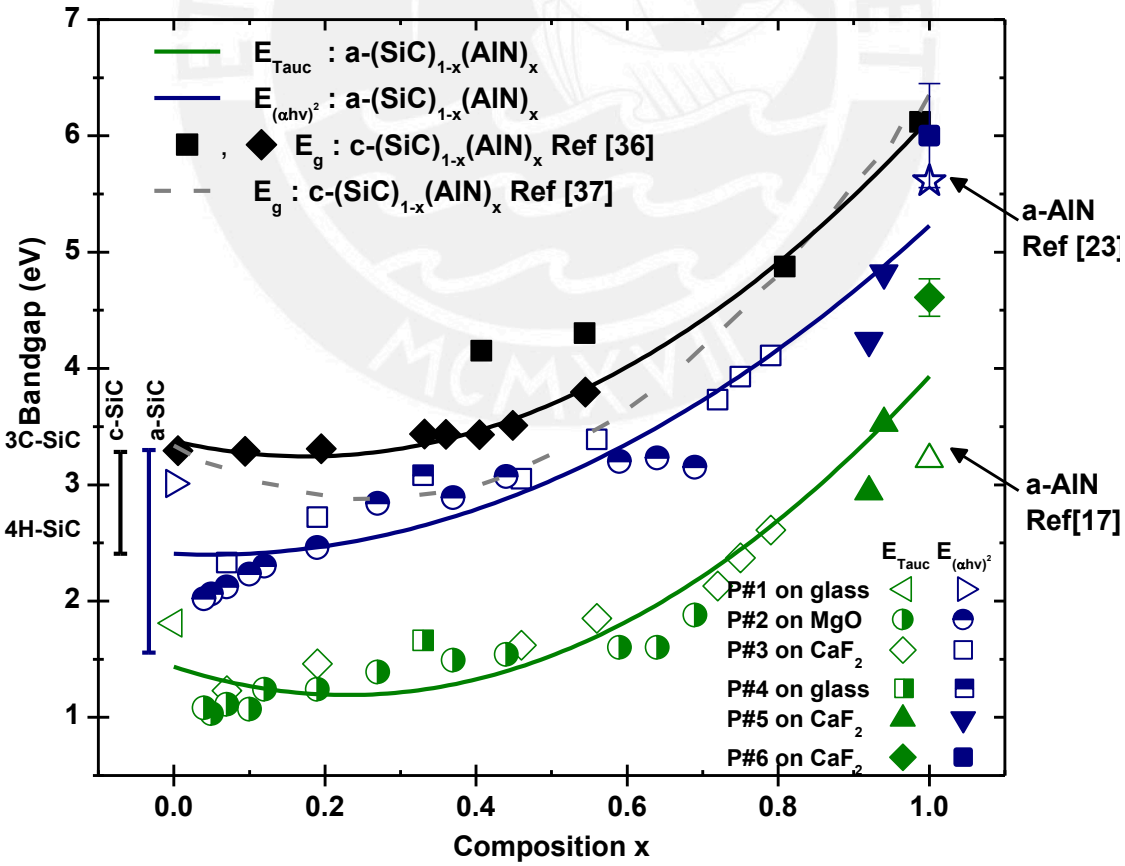

Figure 5.1.1: Optical bandgap versus composition x of a-$(SiC)_{1-x}(AlN)_x$, The Tauc-gap is essentially lower than the $(\alpha hv)^2$ gap. The lines are fitting curves to Vegard's rule of bandgap values of either method. The corresponding fitting parameters are shown in Table 5.1.1. Different film processes are marked by different symbols (denoted by P#). Bandgap values from the literature corresponding to x = 1 are shown. The curve from reference [37] was also included.

The bandgaps obtained with both methods follow Vegard's phenomenological rule, which requires a linear relationship between lattice constants in solid solutions and the composition x. This accounts for a quadratic dependency of the bandgap on the composition x (5.1.1), where b is the bowing parameter, $E_{gap,SiC}$ is the bandgap of pure SiC and $E_{gap,AlN}$ the bandgap of pure AlN.

$$E_{gap}(x) = (1-x)E_{gap,SiC} + xE_{gap,AlN} + bx(1-x) \qquad (5.1.1)$$

Bandgaps of films with a higher SiC content showed a higher deviation from the fitted curve according to Vegard's rule. This could be attributed to possible different hybridization states of the carbon atom in our films since the sputtering processes were slightly different and this may lead to a variation in local structure.

Table 5.1.1. Fitting parameters of Vegard's rule (eq. 5.1.1). The bandgap values of a-SiC and a-AlN and the bowing parameter b are shown for the Tauc and the $(\alpha hv)^2$ plots and for two references.

	Ref[37]	Ref[36]	Tauc method	$(\alpha hv)^2$ method
$E_{gap,SiC}$ [eV]	3.31	3.37±0.05	1.43±0.13	2.40±0.15
$E_{gap,AlN}$ [eV]	6.42	6.14±0.06	3.93±0.17	5.22±0.21
b [eV]	-6.36	-4.26±0.3	-4.61±0.72	-3.11±0.77

Thin films deposited on glass substrates were annealed up to 500°C and the fit to Vegard's rule was performed for each annealing step considering the Tauc-gap only. The resulting behavior is shown in the figure (5.1.2). A significant increase of the Tauc-gap for samples with a high SiC content is observed. These changes registered in the bandgaps might be attributed to a particularly strong reduction of the tail states in the rich SiC region. After the last annealing step at 500°C the parameters according to Vegard's rule are: $E_{gap,SiC}$ = 2.13 eV, $E_{gap,AlN}$ = 3.11 eV and b = -2.72 eV. The absolute bandgap values match well the ones found earlier.

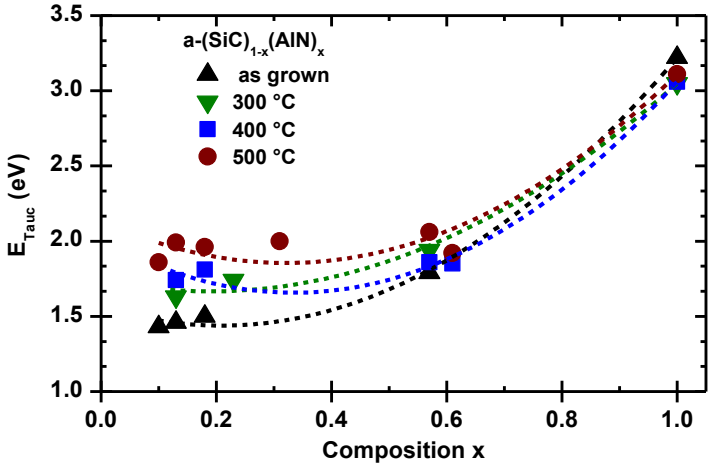

Figure 5.1.2: Tauc-gap versus composition of *a*-$(SiC)_{1-x}(AlN)_x$ thin films deposited on glass substrates. The films were annealed up to 500°C and a clear enhancement of the bandgap in the higher SiC content region is observed. The Tauc-gap values for $x = 1$ were taken from [17].

Urbach tail variation

The significantly change of the bandgap in the SiC region shown in the figure (5.1.2) might be attributed to a strong reduction of the band tail states due to the annealing treatment. To test this argument, annealing treatments up to 700 °C of *a*-$(SiC)_{1-x}(AlN)_x$ samples deposited on MgO substrates were performed. The analyzed compositions were of 80% and 4% AlN and the results of the absorption coefficients of each one are shown in the figure (5.2.1).

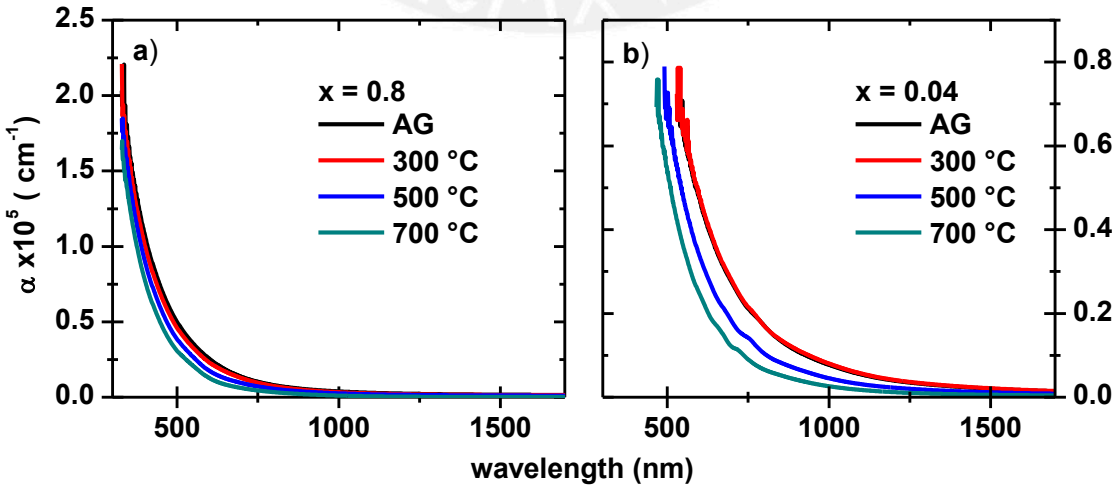

Figure 5.2.1: Absorption coefficients for a film with composition *x* = 80% (a) and for a film with a composition x = 4% (b) for three different annealing temperatures. It is possible to see the strong reduction of the Urbach tails in the SiC rich case.

After an annealing at 300 °C for 30 min, the obtained absorption coefficient from the samples did not present a considerable change, but after 500 °C the variation of the tails is considerable in the rich SiC region in comparison with the rich AlN region. This can be expressed in terms of the disorder energy $1/\beta$ shown in the inserted graph in the figure (5.2.2) where for the AlN rich region an almost linear change is observed, and for the SiC rich region a strong change is observed in comparison.

An explanation to this behavior might be that the amorphous structure in the material as grown is in strain due to the short and long bonds consequence of the topological disorder. With the annealing treatment the atoms have at certain point enough energy to mobilize and therefore a change in the structure is expected. However the structure is still amorphous, but less disordered. In this sense we attribute the reduction of the tails due to annealing treatments as a reduction of the disorder in an as grown material, in agreement with the reduction of the disorder energy shown in the figure (5.2.2).

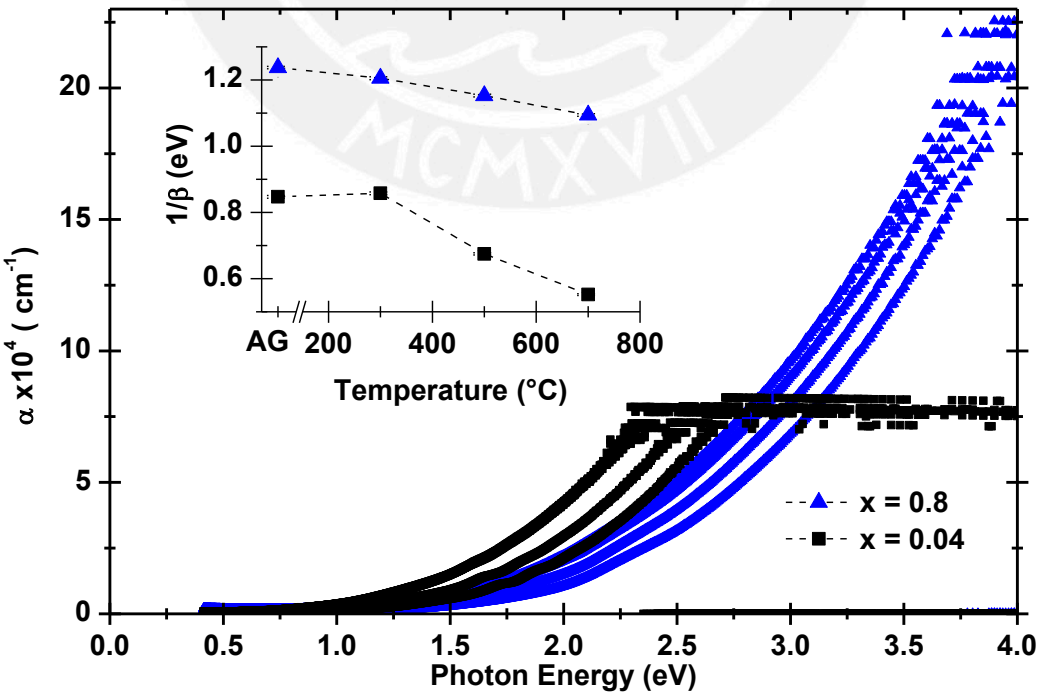

Figure 5.2.2: Absorption coefficients of a-$(SiC)_{1-x}(AlN)_x$ at different annealing temperatures for two compositions blue triangles x = 0.8 and black squares x= 0.04 and their respective disorder energies versus annealing temperatures in the inserted graph. It is possible to see how the band tails are significantly reduced in the SiC rich case in agreement with the results shown in the figure (5.1.2).

To complement this study we apply the Cauchy-Urbach model. A whole new set of pure a-AlN films was evaluated. The absorption coefficient was obtained with the manipulation method proposed in this thesis. The bandgap was determined using the two common representations and the Cauchy-Urbach model for the absorption coefficient. Typical absorption coefficients versus annealing temperatures are shown in the figures (5.2.3) and (5.2.4). It is necessary to remark that as reported in [17] the annealing treatment generate small pin holes in the samples. These pin holes where a problem in some cases for further calculations at temperatures greater than 500°C.

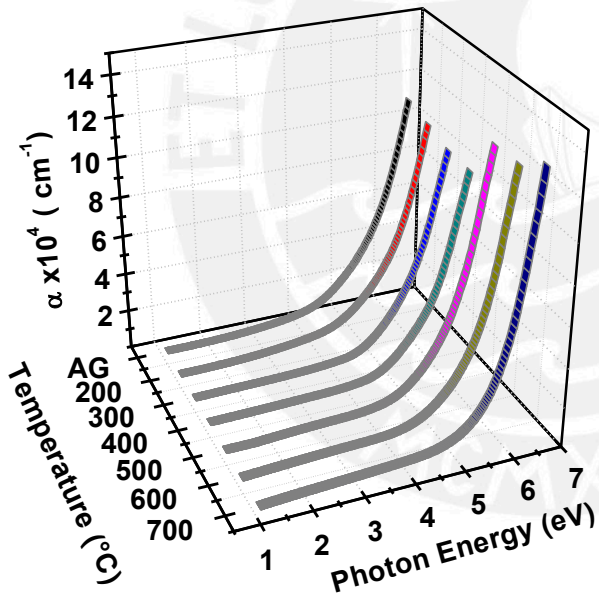

Figure 5.2.3: Absorption coefficient versus energy for each annealing temperature of an a-AlN film with thickness 330.04 ± 0.48 nm. The optical constants and thickness were found by the Manipulation method proposed in this thesis.

Like in the case treated before, it is possible to observe the reduction of the Urbach Tails with the annealing treatment for each increasing temperature. The absorption coefficients were fitted by a global fit sharing the parameters E_0 and α_0 for each sample, the results corresponding to this fit are shown in the figure (5.2.4).

The meaning of this parameter's sharing can be understood in the following way. First, the parameter E_0 is in fact a material constant that does not depend on the structure. Second, both parameters E_0 and α_0 are linked as shown in the equation (4.3.5) by the term $[\ln(\alpha_0) - \beta E_0]$ being the intercept in the logarithm scale of the absorption coefficient and therefore a constant for each absorption curve. By sharing them we are

enforcing that the change of the intercept is only due to a change in the slope and therefore all the absorption curves share a point usually called Urbach focus [6][12][16]. The Urbach focus is normally obtained directly from the Urbach rule [12]. In our case since we are not using the Urbach rule but the Cauchy-Urbach model to fit the absorption coefficient, the Urbach focus can be easily found as $\alpha_f = \alpha_0 \times E_0$ and $E_f = E_0$. In this sense both parameters define the Urbach Focus and it is unique. Therefore the global fit is justified since the material has a defined Urbach Focus no matter the disorder energy. We do the fit for the absorption coefficients at different annealing temperatures corresponding to the same sample in study.

After the fit, the optical bandgap using the Cauchy-Urbach model can be found by the equation (4.3.4). This optical bandgap is in apparent disagreement with the calculated bandgaps using the Tauc representation and the $(\alpha E)^2$ representation shown in the figure (5.2.5). The bandgap obtained using the Cauchy-Urbach model can be considered as another representation of the true gap.

This evaluation was performed for several *a*-AlN samples with a thickness around 300 nm. The Tauc-gaps of these samples are compared in the figure (5.2.6) with the Tauc gap from reference [17]. The resulting bandgaps of four *a*-AlN samples are shown in the figure (5.2.7).

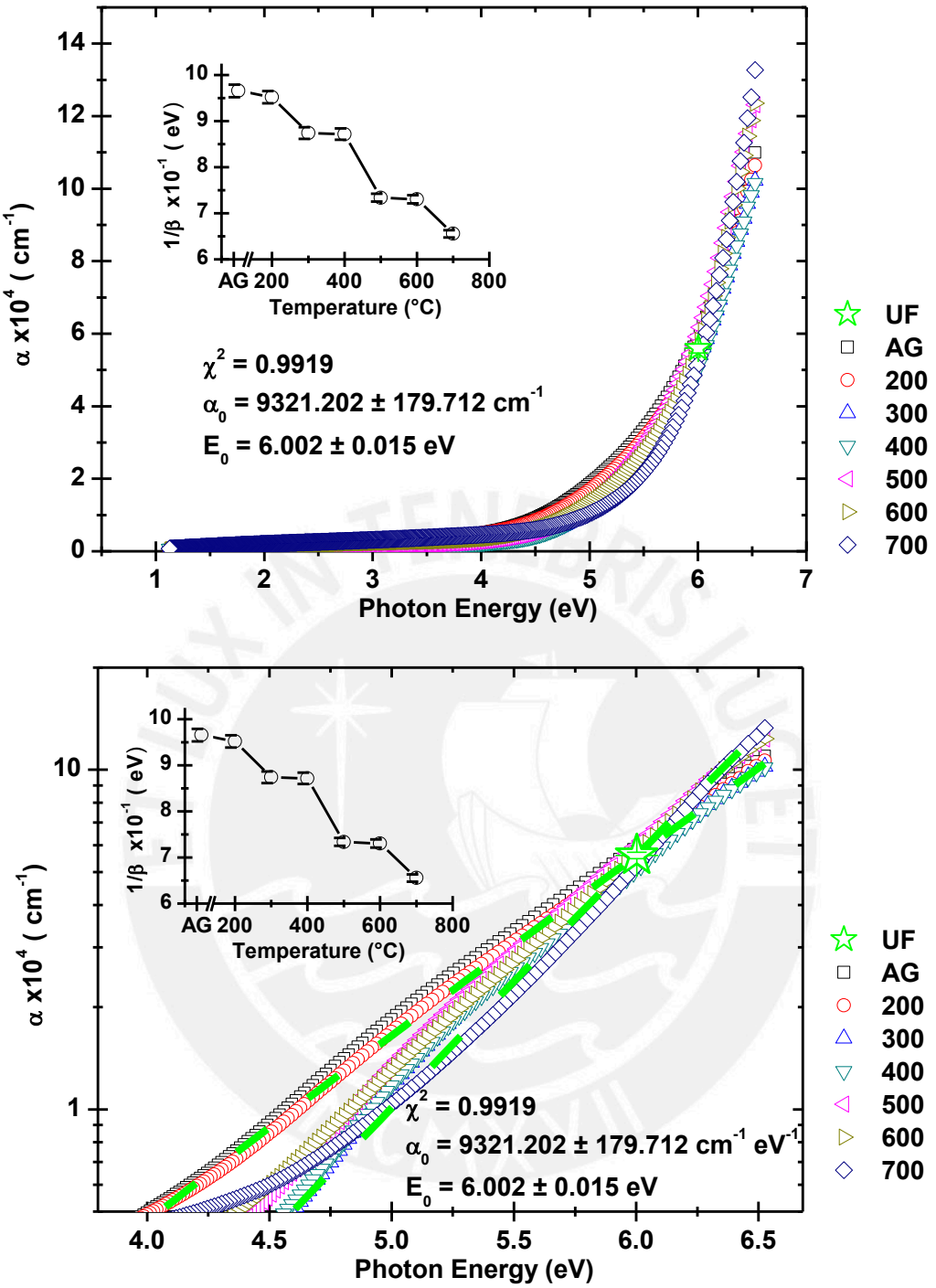

Figure 5.2.4: Absorption coefficients versus photon energy corresponding to each annealing temperatures. The resulting values from the Cauchy-Urbach model fit are shown. The obtained disorder energy is shown in the inset. The value denoted by UF (green star) corresponds to the Urbach focus of the absorption coefficients set shown. It is possible to observe how the slope in the fundamental absorption is increasing with the annealing temperature or disorder (tail) reduction.

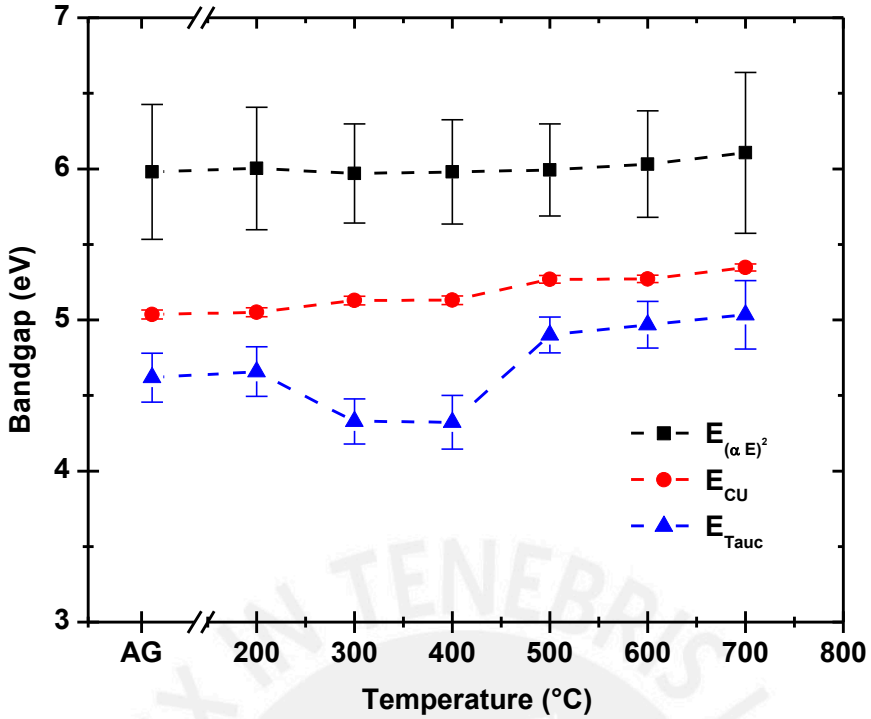

Figure 5.2.5: Comparison between the Tauc-gap E_{Tauc}, $(\alpha E)^2$-gap $E_{(\alpha E)^2}$, and Cauchy-Urbach-gap E_{CU}, versus the annealing temperature corresponding to the absorption coefficient shown in the figure (5.2.4)

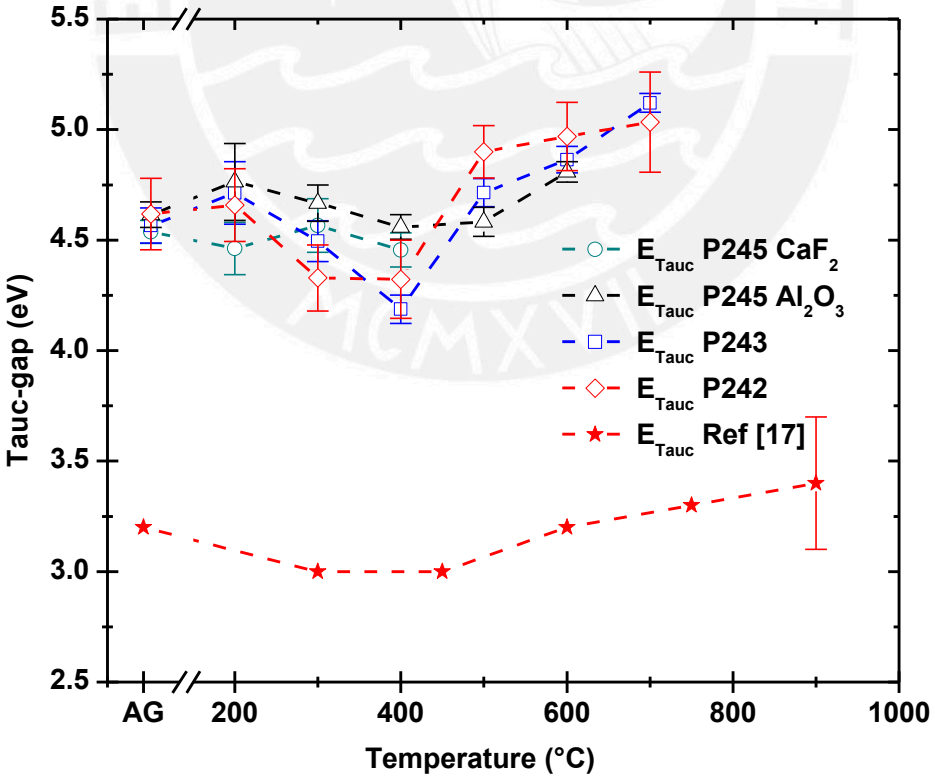

Figure 5.2.6: Tauc-gaps of several samples prepared in our labs, compared with the Tauc-gaps from reference [17]. The disagreement with the reference [17] might be attributed to the amount of data close to the fundamental absorption, our samples where thinner and therefore the absorption coefficient data was closer to the fundamental absorption.

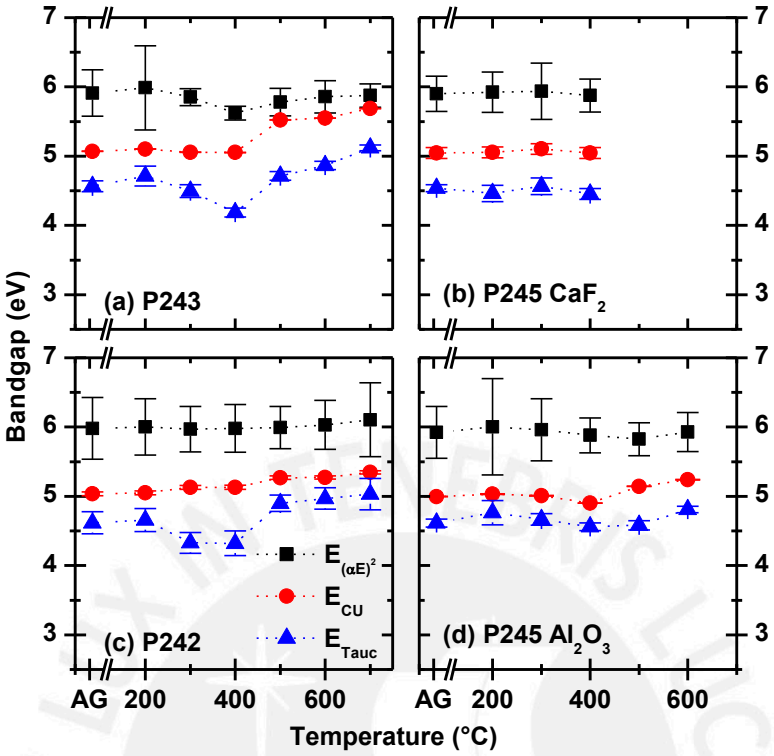

Figure 5.2.7: Comparison between the three different methods for obtaining the optical bandgap of four *a*-AlN thin films with thicknesses around 300 nm.

Conclusions

A method to determine the optical constants of thin amorphous films with a low interference transmission spectrum was developed and implemented. This method was used to determine the optical bandgap of *a*-$(SiC)_{1-x}(AlN)_x$ thin films for compositions in the whole range. The enhancement of the optical bandgap and the reduction of the band tails due to annealing treatments were studied. The mean value of the obtained Urbach focus of pure *a*-AlN films is $\langle \alpha_f \rangle = 96775.81 \pm 3178.46\ \text{cm}^{-1}$ and $\langle E_f \rangle = 6.17 \pm 0.03$ eV. The E_f value corresponds to the bandgap of the material in the crystalline state.

The results of this work were published in [3][4][5]. The developed method was used to determine the thickness of several samples in order to determine the deposition rate pattern of the magnetrons without damaging the samples and the corresponding results were published in [24][25].

References

[1] A.J. Steckl and J.M. Zavada, MRS Bull. 24 (1999), 16.

[2] K. Gurumurugan, H. Chen, G. R. Harp, W. M. Jadwisienczak, H. J. Lozykowski: A. Phys. Lett. Vol. 74 (1999), 3008.

[3] R. Weingärtner J. A. Guerra, O. Erlenbach, G. Gálvez, F. De Zela, R. Weingärtner A. Winnacker, Mater. Sci. Eng. B (2010), doi:10.1016/j.mseb.2010.03.033

[4] J. A. Guerra, A Wintersein, O. Erlenbach, G. Galvez, F. De Zela, R. Weingärtner, A. Winnacker, Materials Science Forum Vols. 645-648 (2010), 263-266.

[5] O. Erlenbach, G. Gálvez, J. A. Guerra, F. De Zela, R. Weingärtner, A. Winnacker, Materials Science Forum Vols. 645-648 (2010), 459-462.

[6] Singh J., Shimakawa K. *Advances in amorphous semiconductors* (T&F, 2003).

[7] J. Tauc, Res. Bull. Vol. 3 (1968), 37.

[8] Levine, Ira N., *Quantum chemistry* (Upper Saddle River, N.J.: Prentice Hall, 2000)

[9] Yu Cardona, *Fundamentals of Semiconductors* (Springer 3rd Edition, 2004)

[10] Krane, K., *Modern Physics* (Wiley, New York 1996)

[11] R. Zallen, *The physics of amorphous solids*, (Wiley, 1983)

[12] Kazuo Morigaki, *Physics of amorphous semiconductors* (Imperial College Press, 1999)

[13] Cohen Tannoudji, *Quantum mechanis* (París: Wiley, 1977)

[14] Mott, Nevill F., *Electronic processes in non-crystalline materials* (Oxford: Clarendon Press, 1971)

[15] L. L. Moseley, T. Lukes, Am. J. Phys. Vol. 46 (1978), 676.

[16] S. R. Elliot *Physics of amorphous materials*, (Longman Scientific & Technical, 1990)

[17] A. R. Zanatta, J. Phys. D: Appl. Phys. Vol. 42 (2009), 025109.

[18] D. J. Dunstan, J. Phys. C: Solid State Phys., Vol. 16 (1983), L567-L571.

[19] D. J. Dunstan, J. Phys. C: Solid State Phys., Vol. 18 (1985), 5429.

[20] T. Skettrup, J. Phys. Rev. B, Vol 18, (1978), 2622.

[21] A. K. Ray and C. A. Hogarth, J. Phys D: Appl. Phys., Vol. 23, 458.

[22] J.M. Khoshmana & M.E. Kordesch, Journal of Non-Crystalline Solids, 351 (2005), 3334.

[23] Sadao Adachi, *Optical properties of crystalline and amorphous semiconductors*, (Kluwer Academic Publishers, 1999)

[24] G. Gálvez, O. Erlenbach, J. A. Guerra Torres, T. Hupfer, M. Steidl, F. De Zela, R. Weingärtner, A. Winnacker, Materials Science Forum Vols. 645-648 (2010), 1199-1202.

[25] G. Gálvez, J. A. Guerra Torres, O. Erlenbach, M. Steidl, F. De Zela, R. Weingärtner, A. Winnacker, Mater. Sci. Eng. B (2010), doi:10.1016/j.mseb.2010.03.012

[26] Griffiths D.J., *Introduction to electrodynamics* (3ed., PH, 1999).

[27] Swanepoel R., J. Phys. E:Sci Instrum., Vol. 16 (1983).

[28] Manifacier J C, Gasiot J and Fillard, J. Phys. E: Sci. Instrum. Vol. 9 (1976), 1002-4.

[29] G. A. N. Connel and A. S. Lewis Phys. Status Solidi B, Vol 60 (1973), 299.

[30] E. R. Shaaban, J. Phys. and Chems. of Solids, Vol 68 (2007), 400.

[31] E. Márquez *et all*, J. Phys. D: Appl. Phys., Vol 25 (1992), 535.

[32] J. B. Ramírez *et all*, Phys. Stat. Sol., Vol 133 (1992), 499.

[33] Hong Chen, Appl. Phys. Lett., Vol 77, 8 (2000), 1117.

[34] D. Poelman & P. F. Smet 2003 Phys. D: Appl. Phys. Vol. 36, 1850-57.

[35] V. A. Dmitriev, *Amorphous and Crystalline Silicon Carbide III* (Springer, 1990), Vol. 56, 3.

[36] Sh. A. Nurmagomedov, Sov Tech Phys Lett. Vol. 12 (1986), 431.

[37] R. Roucka, J. Tolle, A. V. G. Chizmeshya, P. A. Crozier, C. D. Poweleit, D. J. Smith, J. Kouvetakis, I. S. T. Tsong: Applied Surface Science Vol. 212-213 (2003), 872.

[38] Neil W. Ashcroft, N. David Mermin, *Solid State Physics* (1976).